European Journal of Pharmaceutics and Biopharmaceutics 134 (2019) 1–19

Contents lists available at ScienceDirect

European Journal of Pharmaceutics and Biopharmaceutics

journal homepage: www.elsevier.com/locate/ejpb

Research paper

Betulin silver nanoparticles qualify as efficient antimelanoma agents in *in vitro* and *in vivo* studies

Corina Danciu[a,1], Iulia Pinzaru[a,1], Dorina Coricovac[a,*], Florina Andrica[a], Ioana Sizemore[b], Cristina Dehelean[a], Flavia Baderca[c], Voichita Lazureanu[c], Codruta Soica[a], Marius Mioc[a], Heinfried Radeke[d]

[a] Faculty of Pharmacy, "Victor Babes" University of Medicine and Pharmacy, 2nd Eftimie Murgu Sq., Timisoara 300041, Romania
[b] Department of Chemistry, Wright State University, Dayton, OH 45435-0001, USA
[c] Faculty of Medicine, "Victor Babes" University of Medicine and Pharmacy, 2nd Eftimie Murgu Sq., Timisoara 300041, Romania
[d] Institute of Pharmacology and Toxicology Clinic of the Goethe University Frankfurt Main, D-60590 Frankfurt Main, Germany

ARTICLE INFO

Keywords:
Betulin silver nanoparticles
Melanoma
C57BL/6J mice
Histopathological assessment
B16 melanoma 4A5
B16Ova

ABSTRACT

The current study was purported to assess the: (i) *in vitro* toxicity of betulin silver nanoparticles (AgNPs-B), bare and capped with polyethylene glycol (PEG), on two murine melanoma cell lines (B164A5 and B16Ova) and on healthy cell lines (keratinocytes and melanocytes), and (ii) *in vivo* antitumor efficacy of PEGylated AgNPs-B in an experimental melanoma model. Bare and PEG-capped AgNPs-B were synthesized by a chemical reduction method resulting in stable and non-aggregated spherical AgNPs-B and PEG-AgNPs-B, of narrow size distributions and mean hydrodynamic diameters of 25 nm and 75 nm, respectively. *In vitro* assessments were achieved by MTT and Annexin V-FITC assays and *in vivo* evaluation involved non-invasive techniques for the surveillance of the physiological skin parameters changes and histopathological examination of the harvested organs. The *in vitro* results revealed selective cytotoxicity against melanoma cells, at low doses that are nontoxic to normal cells; higher doses were associated with the loss of selectivity and toxicity for healthy cells. PEGylated formulation of betulin exerted a dose-dependent pro-apoptotic effect, more obvious in the case of B164A5 cells. Histopathological analysis suggested that PEGylated AgNPs-B developed relevant *in vivo* effects as antimelanoma agents by decreasing the tumor volume and inhibiting the development of secondary tumors.

1. Introduction

Melanoma is considered a multietiologic disorder and a major health problem worldwide in the light of an increased incidence, aggressiveness and high costs needed for prevention, diagnosis and treatment. Although it is less common compared to other skin cancers, melanoma is the most aggressive among all types of cutaneous cancer and the survival rate depends on several factors (stage, age, sex etc.). Moreover, it proved to have an advanced metastatic potential and a significant resistance to chemotherapy leading to a high death rate [1]. More than 90% of deaths from skin cancers are caused by melanoma. To give an overview of the respective survivals rates: nearly 100% survival at 10 years if identified in early stages and treated by surgical excision; 63 and 50% survival after 10 years, for stage III and IV melanoma, respectively, if treated by systemic interventions which are aggressive and partially efficacious with the remark that for stage IV melanoma the average survival time is 9 months [2,3]. The risk of developing the disease is related to both genetic/phenotype and environmental/exposure factors, such as: sun exposure, pigmentary characteristics (hair, eye, and skin color), number of naevi, immunosuppression, family history of melanoma, and environmental exposures [4].

At present, five types of standard treatment are approved and applied for melanoma patients, namely: surgery, radiation, chemo-, immune-, and targeted therapies, which despite countless discoveries about melanoma treatment, remain aggressive, laborious and very expensive [5,6]. Melanoma has been the prime example of successful therapies with so-called check-point inhibitors in recent years,

* Corresponding author.
E-mail addresses: corina.danciu@umft.ro (C. Danciu), iuliapinzaru@umft.ro (I. Pinzaru), dorinacoricovac@umft.ro (D. Coricovac), ioana.pavel@wright.edu (I. Sizemore), cadehelean@umft.ro (C. Dehelean), codrutasoica@umft.ro (C. Soica), marius.mioc@umft.ro (M. Mioc), radeke@em.uni-frankfurt.de (H. Radeke).
[1] Authors that contributed equally.

https://doi.org/10.1016/j.ejpb.2018.11.006
Received 12 April 2018; Received in revised form 23 October 2018; Accepted 5 November 2018
Available online 07 November 2018
0939-6411/ © 2018 Elsevier B.V. All rights reserved.

comprising antibodies towards immune suppressive, co-inhibitory membrane molecules like CTLA4 and PD-L1 [7,8]. Nevertheless, albeit the results are promising, the percentage of cancer patients responding to treatment is limited. Moreover, as with conventional, synthetic/chemical drugs used for melanoma, the immune check-point inhibitor treatment is hampered by multiple serious side effects and resistance [9]. Therefore, thorough studies with reference to biologically active compounds of natural origin remain of high interest. This type of compounds has several advantages as low or devoid of toxicity, low cost and frequent use in the form of natural medicines or dietary supplements [6]. Also, these compounds exhibited adjuvant properties that in combination may support re-activation of anticancer immunity [10].

Betulin [betulinol, lup-20(29)-ene-3β,28-diol] belongs to the class of pentacyclic triterpenes and is the predominant compound of the outer bark of the *Betula* birch tree with notable biological properties, such as anti-cancer, anti-bacterial, anti-inflammatory, anti-fungal, and anti-viral, effective on lesions and severe skin damage, as both prophylactic and curative agent [11]. Its activity related to skin diseases is outstanding mostly due to the multitargeted mechanism of action, as follows: (i) acts as a suppressor of superoxide generation preventing tyrosyl phosphorylation of a 45 kDa-protein in human neutrophils, (ii) targets membrane melanocortin receptors which are expressed in the skin as well as in melanoma and immune cells and (iii) exerts inhibitory activity against different melanoma and skin cancer cell lines and anti-angiogenic activity [1,12]. Despite these beneficial properties, the use of betulin *in vivo* is restricted due to some major disadvantages namely reduced solubility and stability [12,13]. Finding suitable formulations to increase the solubility and stability of this molecule without affecting its pharmacological properties is still a challenge for researchers in the field.

Metallic nanoparticles, recognized as “theranostic” compounds due to their ability to exert diagnostics and treatment properties, represent a solution for stabilizing and targeting biologically active molecules. Silver nanoparticles (AgNPs) possess prophylactic environmental and antibacterial effects and were proved to have anticancer effects, due to the capacity to generate DNA damage, chromosomal aberrations, cell cycle arrest, oxidative stress, apoptosis and necrosis [14,15]. Pinzaru *et al.* obtained both, stable, non-aggregated spherical silver nanoparticles and PEGylated silver nanoparticles (PEG-AgNPs) to use them as carriers for agents with low aqueous solubility administered in skin pathologies and had proven that these formulations are applicable in certain doses on biological studies [15].

Preclinical studies aiming to understand the etiology and mechanisms involved in the occurrence and progression of malignant diseases and to assess the effectiveness of new therapies imply most frequently xenograft, syngeneic, and genetically engineered animal models [5,16]. Transplantable murine melanomas are well-established tools for the assessments of different compounds with anti-cancer properties. B16 is a murine melanoma cell line obtained for the first time in 1954 in Jackson Laboratories in Maine from a malignant melanocytic tumor developed spontaneously in a C57BL/6 mouse, marking the starting point for the generation of other B16 sublines. B16 melanoma 4A5 is one of the most widely used cell lines for the murine melanoma model, presenting fibroblast-like characteristics and the ability to produce melanin [16–18]. Murine B16Ova melanoma cells (H2-Kb) are derived from a B16.F1 clone transfected with a pcDNA3.1ova plasmid [19,20].

The research presented here provides relevant data considering: (i) the development and characterization of betulin-loaded, bare and PEGylated silver nanoparticles, (ii) evaluation of the cytotoxic and anti-proliferative properties of the compounds on normal keratinocytes and melanocytes and on tumor cells (B16 melanoma 4A5 and B16Ova), and (iii) assessment of the *in vivo* behavior of PEGylated formulations (with and without betulin) on a murine melanoma model based on skin parameters and histopathological analysis.

2. Materials and methods

2.1. Reagents and cell lines

The reagents used in the present study, such as: silver nitrate (Merck, Germany), trisodium citrate (Sigma-Aldrich, Germany), sodium lauryl sulfate, (Acros Organics, Belgium), polyethylene glycol (PEG-400) (Sigma-Aldrich, Germany), and betulin (Sigma-Aldrich, Germany) were of analytical grade and used without any purifying step. Solvents utilized throughout the experiments were Milli-Q water, methanol and dimethyl sulfoxide – DMSO (Sigma Aldrich, Germany). The highest concentration of DMSO in the medium did not exceed 0.1% and had no influence on the parameters evaluated in all experiments presented.

The reagents applied for the *in vitro* tests were acquired from Sigma Aldrich (Munich, Germany): fetal calf serum (FCS), saline phosphate-buffered (PBS), penicillin/streptomycin mixture, trypsin-EDTA solution, from Gibco (Karlsruhe, Germany): Dulbecco's Modified Eagle's Medium (DMEM), HEPES 4-(2-hydroxyethyl)-1 piperazine-ethane-sulfonic acid, and from ATCC (American Type Culture Collection): Dermal Cell Basal Medium and Adult Melanocyte Growth Kit. The MTT Cell Proliferation Assay Kit was purchased from Roche Applied Science (Mannheim, Germany), Annexin V-fluorescein from ImmunoTools GmbH (Oldenburg, Germany), 7-Amino-actinomycin D (7-AAD) from eBioscience (Germany), and staurosporine from LC Laboratories (Woburn, USA).

The cell line B16 melanoma 4A5 was purchased from Sigma-Aldrich Chemie GmbH (Munich, Germany) (94042254) and the cell line B16Ova was received as a gift from Prof. Dr. Med. Heinfried Radeke, Department of Pharmacology, Immunology, Universitätsklinikum Goethe, Frankfurt, Germany. The healthy cell lines: HEMa – primary epidermal melanocytes (ATCC® PCS-200-013™) and HaCat – immortalized human keratinocytes were obtained from ATCC.

2.2. Preparation and physicochemical characterization of silver colloids

AgNPs were prepared using a slightly modified Turkevich’s process [21]. Briefly, an aqueous solution of silver nitrate (1 mM) was added under continuous stirring to a solution of trisodium citrate (0.4 mM) and sodium lauryl sulfate (0.5 mM) over a period of 30 min, and the reaction mixture was kept at temperature until the formation of a yellow pale characteristic color. An aqueous solution of polyethylene glycol (PEG 400) was dropped under continuous stirring to the AgNP colloid, to obtain PEG-capped AgNPs. Bare or PEG-capped betulin AgNP colloids (AgNPs-B and PEG-AgNPs-B) with a final concentration of 0.02 mM have been synthetized by adding dropwise and with continuous stirring a liquid form of betulin in methanol to the previously obtained AgNP and PEG-AgNP colloids. The resulting colloids were kept at cold and were protected from light.

To confirm the formation of nanoparticles, standard physicochemical measurements such as UV–Vis absorption spectrophotometry (Cary 60 UV–Vis spectrophotometer, 200–600 nm domain) and Raman spectroscopy (LabRam HR 800 system, confocal Raman microscope – BX41, a 50x Olympus objective, a He-Ne laser, 15 mW output, a thermoelectrically cooled CCD camera) were carried out. The morphology, dimensions and stability of AgNPs were assessed by TEM (FEI Tecnai 12 Biotwin microscope) and zeta analysis (Zetasizer Nano ZS system, Malvern Instruments, Malvern, UK).

2.3. Drug loading capacity and encapsulation efficiency

A betulin solution in methanol (1 mM) was prepared, analyzed by UV–Vis spectrophotometer (Cary 60 UV–Vis spectrophotometer, 190–400 nm domain) and used as control. The substance showed a maximum absorption wavelength at 210 nm and the calibration curve was achieved by applying various dilutions (in the range 0.05–0.5 mM). The drug loading capacity, corresponding to AgNPs-B and PEG-AgNPs-

B, respectively, in a mass ratio of 1:1, was determined by two methods: (1) indirectly, by assessing the drug content in the supernatant and (2) directly, by evaluating the drug content present in the drug sediment resulted after centrifugation. The drug concentration either in the supernatant or in the re-dispersed drug sediment was determined at 210 nm wavelength.

The drug loading capacity (LC) and encapsulation efficiency (EE) were calculated by the following formulas [22].

$$\text{Loading efficiency (LC)} = \frac{W_t - W_s}{W_{NP}} \times 100\,\% \quad (1)$$

$$\text{Encapsulation efficiency (EE)} = \frac{W_t - W_s}{W_{NP}} \times 100\,\% \quad (2)$$

were:

W_{NP} = quantity of silver nanoparticles added

W_t = total amount of drug added

W_s = drug quantity in the supernatant, spectrophotometrically determined

2.4. Cell culture

The B16 melanoma 4A5, B16Ova and HaCat cells were cultured in specific culture medium – Dulbecco's modified Eagle Medium (DMEM) supplemented with 2% Hepes 4-(2-hidroxietil)-1-piperazineethanesulfonic acid, 2 mM L-glutamine, 1% penicillin/streptomycin 10,000 UI/mL and 10% fetal calf serum (FCS). HEMa cells were cultured in Dermal Cell Basal Medium supplemented with an Adult Melanocyte growth kit, 1% penicillin/streptomycin mixture and 1% FCS. Cells were kept in a humidified atmosphere with 5% CO_2 at 37 °C and were passaged every other day. Countess™ II Automated Cell Counter and Trypan blue were used to establish the number of cells for the tests.

2.5. Cell viability and proliferation assays

The viability test applied in the present study was MTT (3- (4,5-Dimethylthiazol-2-yl)-2,5-diphenyltetrazolium bromide) assay. B16Ova and B16 melanoma 4A5 cells (6×10^3 cells/well) were seeded in a 96 well microplate (100 µL/well) using DMEM with 10% FCS and allowed to attach. In the case of HaCat and HEMa cells, 10^4 cells/well was considered to be the optimum number based on previous tests [15,23]. After 24 h, a new medium containing 1% FCS (100 µL/well) was added and the cells were stimulated with different concentrations of the tested compounds (0, 0.5, 1, 5, 15, 30, 50 and 100 µM) for 72 h. The MTT reagent (10 µL) was added and incubated for 4 h. The resulting purple crystals were dissolved in a solubilization buffer (100 µL/well) and the samples were spectrophotometrically analyzed at 570 nm, using a microplate reader (SpectraMaxM5e). The data were presented as the mean % of viable cells compared to the control ± SD, n = 3 for each concentration. Betulin was considered as positive control using the same concentrations as test compounds. The IC_{50} value was calculated using GraphPad Prism version 5.00, GraphPad Software.

Apoptosis was evaluated by using Annexin V-FITC staining. The cells were cultivated for 24 h with different concentrations between 0.5 and 100 µM of test compounds (silver colloids). A number of 1×10^6 cells were incubated with 5 µL of Annexin V-fluorescein and 5 µL of 7-Amino-actinomycin D (7-AAD) in a scheduled buffer for 15 min and then analyzed by flow cytometry on FACS Canto II system (BD Biosciences, Heidelberg, Germany) using a FACS DIVA device. The DMSO treated cells were used as negative control, and the cells treated with 500 nM staurosporine were used as positive control.

2.6. In vivo toxicity protocol

To obtain the murine melanoma model, C57BL/6J adult female mice (12–14 weeks, weight: 23 ± 2 g, from Charles River Laboratory, Budapest, Hungary) and murine B16 melanoma 4A5 cells were used. The animals were acclimatized to the laboratory conditions for 14 days before the experiment, being hosted in the University animal facility in compliance with standard conditions: a 12 h light/12 h dark cycle, food and water *ad libitum*, ambient temperature between 22 and 24 °C, and humidity around 55%. The experiments were conducted in agreement with the European Directive 2010/63/EU, the AVMA Guidelines for the Euthanasia of Animals (2013 Edition) and the National Law 43/2014 regarding the protection of animals used for scientific purposes and were approved by the University Research Ethics Committee.

The experimental protocol comprises three stages: (a) preparation of B16 melanoma 4A5 cell suspension, 1×10^6 cells/100 µL of PBS/mice, (b) subcutaneously administration of cell suspension in the mice hair-depilated dorsal area and (c) treatment of mice with PEGylated silver colloid suspensions after tumor appearance. The B16 melanoma 4A5 cells were cultured in the similar manner as described above in the cell culture paragraph. The mice were divided in four groups (n = 6 mice/group): group 1 – control group (no interventions were applied); group 2 – mice inoculated with B16 melanoma 4A5 cells; group 3 – mice inoculated with B16 melanoma 4A5 cells and administered 6 doses of PEG-AgNPs, 10 mg/kg body weight, group 4 – mice inoculated with B16 melanoma 4A5 cells and administered 6 doses of PEG-AgNPs-B, 10 mg/kg body weight, at every two days. The mice were monitored daily, and the tumor volume was measured with a caliper and calculated using the formula $V = ba^2/2$, where *a* represents the tumor width and *b* the tumor length.

2.7. Non-invasive assessment

Changes in skin physiological parameters were evaluated using a Multiprobe Adapter System, MPA5 (Courage-Khazaka, Germany), fitted with a specific probe for each parameter, as follows: skin hydration – Corneometer CM 825 (Courage-Khazaka, Germany), transepidermal water loss – Tewameter® TM300 probe (Courage-Khazaka, Germany), and melanin and erythema – Mexameter® MX 18 (Courage-Khazaka, Germany). The skin measurements were done in triplicate every three days.

2.8. Histopathological evaluation

At the end of the experiment, the mice were euthanized under anesthesia followed by cervical dislocation. The techniques used to euthanize the mice were in agreement with AVMA Guidelines for Euthanasia. Clinically normal skin, cutaneous tumor and several organs (heart, kidney, liver, lung, and spleen) were harvested from all animals, weighed, fixed in 4% v/v buffered formaldehyde and embedded in paraffin. Sections of 3 µM thickness were obtained using a Leica rotary microtome RM2255 and dyed with hematoxylin and eosin (H&E) using the standard histopathological method. Microscopic observations were made using a Leica light microscope DM750 and images were captured using a Leica DMShare System.

2.9. Statistical analysis

Origin 8, Graph Pad Prism 5, and Flow Jo (7.6.5) were employed for the description and performance of the data. One-way ANOVA followed by the Bonferroni test was used to determine the statistical differences between the various experimental and control groups. Significant results ($p < 0.05$) between the different groups were denoted as follows: * for $p < 0.05$, ** for $p < 0.01$ and *** for $p < 0.001$. The results were expressed as the means ± standard deviation.

2.10. Compliance with ethics requirements

Researchers involved declare that the experiment implying animals

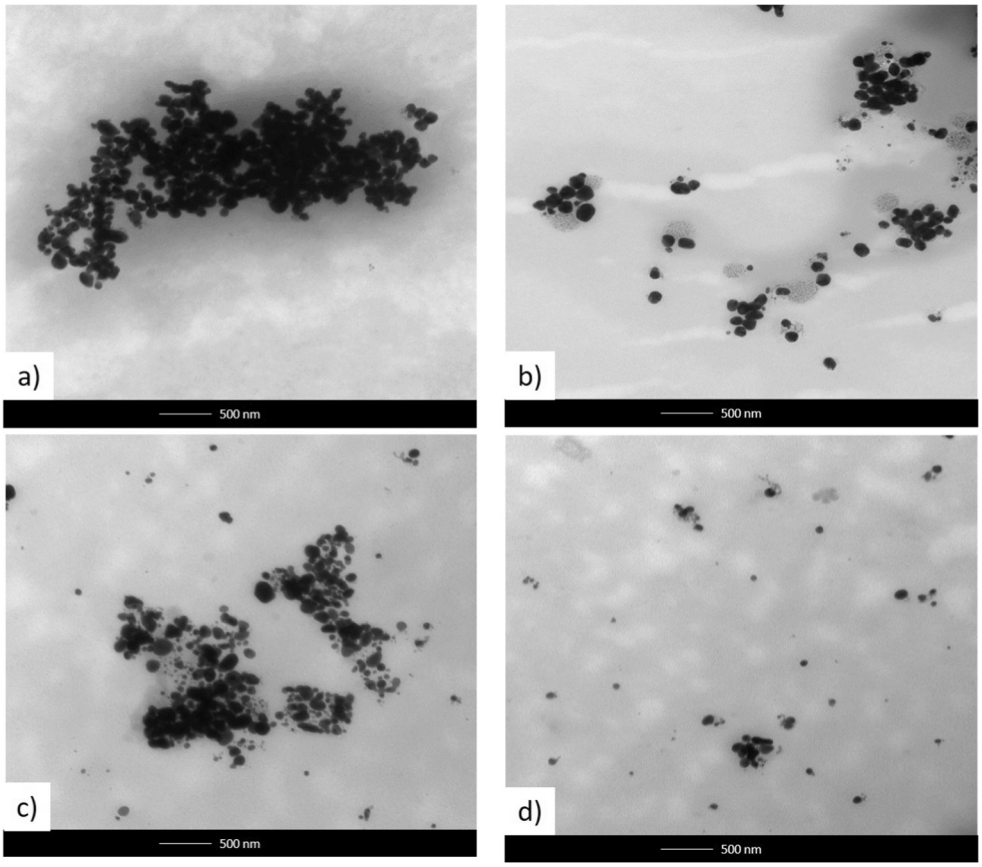

Fig. 1. TEM images of the silver nanoparticles: (a) AgNPs, (b) AgNP-B, (c) PEG-AgNP and (d) PEG-AgNP-B. Scale bars are 500 nm.

for scientific purposes complied with the related legislation; this protocol was analyzed and approved by the Ethics Committee of the "Victor Babes" University of Medicine and Pharmacy Timisoara, Romania.

3. Results

3.1. Physicochemical characterization

Both AgNPs-B and PEG-AgNPs-B were successfully synthetized and characterized. Particle size analysis showed that the silver colloids obtained had broad size distribution (AgNPs-B) and some narrow size distributions (PEG-AgNPs-B) with mean hydrodynamic sizes around 25 nm and 75 nm, respectively. TEM images demonstrated that the majority of AgNPs were spherical and multifaceted (Fig. 1).

The electrostatic stabilization of betulin-loaded, bare and PEGylated silver nanoparticles was evaluated by measuring their zeta potential values. Zeta potential value was found to be in the range of −37.3 (AgNPs) mV to −27.4 (PEG-AgNPs-B) for silver colloids with an average size between 25 and 75 nm (Fig. 2). This can be assigned to extremely high surface energies of nanoparticle suspensions tested in cell medium.

Changes in the profile of the localized surface plasmon resonance (LSPR) peak of AgNPs demonstrate adsorption of betulin to nanosilver surface (Fig. 3). DMSO and water vibrational modes were present in all samples. Vibrational modes characteristic to PEG were observed in all Raman spectra of PEG-AgNPs samples at 830, 1065, 1126, 1244, 1283, 1470, and 2877 cm^{-1} suggesting the PEGylation of AgNPs, while peaks attributed to betulin were detected in both AgNPs and PEG-AgNPs samples at 760, 900, 1018, and 1384 cm^{-1} [24–26] (Table 1, Fig. 4). The experimental and theoretical FT-Raman spectra of free betulin were performed during the present experiment (Fig. 5), being also described thoroughly in a previous study conducted by our group [25] and indicate that betulin was adsorbed onto AgNPs and PEG-AgNPs surface through the $-COO^-$ group. This is confirmed by: (a) the appearance of a new Ag-O stretching mode at 236–238 cm^{-1} [24,26] and (b) the band at 1524 cm^{-1} characteristic to the $-COO^-$ functional group adsorbed to the silver surface [24,26].

Drug delivery represents a process which is directly dependent on loading capacity, also known as payload efficiency. As presented in Table 2, results showed that both methods employed for LC determination provided fairly similar values for both formulations AgNPs-B and PEG-AgNPs-B, respectively.

3.2. Cells viability assessment – MTT

In order to assess the effects induced by AgNPs-B and PEG-AgNPs-B on B16 melanoma 4A5 and B16Ova murine melanoma cells viability, dose-response experiments were conducted employing various concentrations (0, 0.5, 1, 5, 15, 30, 50 and 100 μM) in a 72 h exposure. Betulin, the positive control was also tested in the same experimental conditions, and the results obtained for test compounds (AgNPs-B and PEG-AgNPs-B) were statistically analyzed in rapport with the results of betulin. Betulin proved to be highly toxic for B16 melanoma 4A5 cells at concentrations > 15 μM leading to a viability rate lower than 9% (IC_{50} value = 4.269 μM), the effect being dose-dependent. A similar effect was induced by betulin in the case of B16Ova cells with an IC_{50} value of 3.89 μM (Fig. 6).

The AgNPs-B formulation exerted a strong decrease of B16 melanoma 4A5 living cells percentage even at concentrations as low as 1 μM (around 60%). The decrease induced by AgNPs-B was dose-dependent, concentrations higher than 50 μM being extremely toxic for the cells leading to a viability rate of 5% (Fig. 6). The IC_{50} value was 0.9301 μM, a value lower than the one obtained for betulin (4.269 μM), what

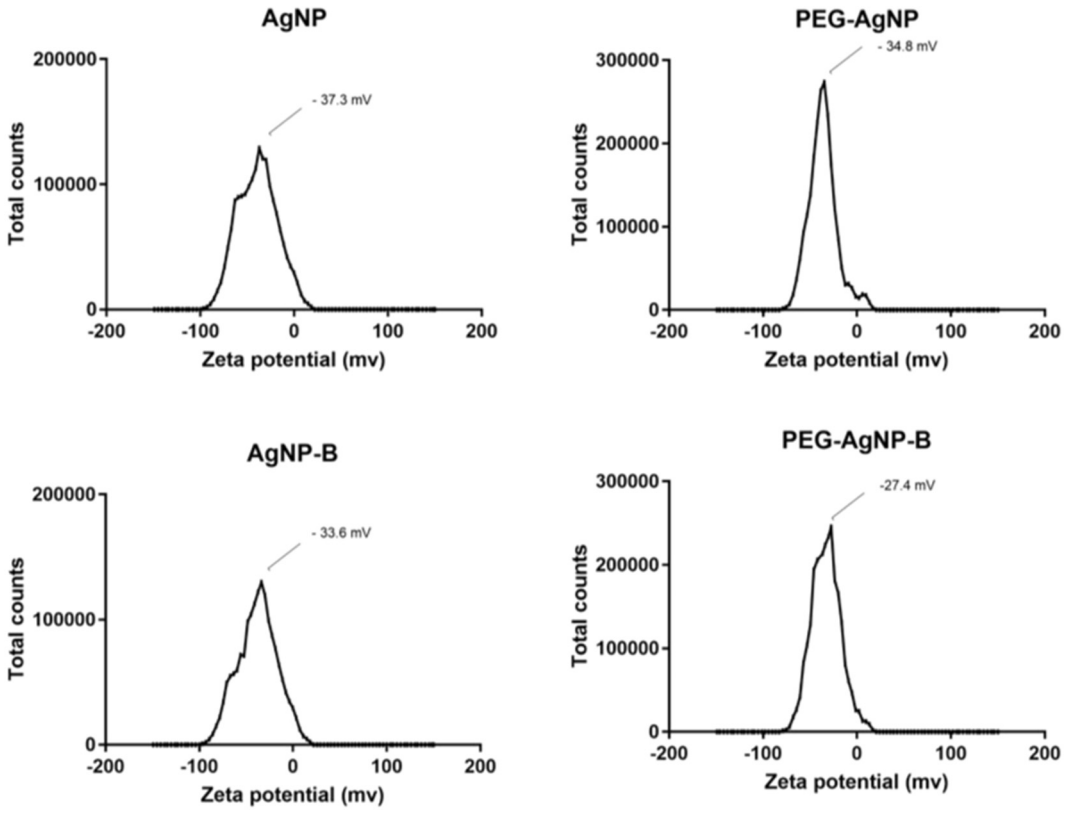

Fig. 2. Zeta potential values recorded for betulin-loaded, bare and PEGylated silver nanoparticles.

proves the potent inhibitory effect of AgNPs-B on B16 melanoma 4A5 cells viability. The evaluation of bare AgNPs also showed a reduced viability percentage, but the viability rate (%) of B16 melanoma 4A5 cells started to significantly decrease at concentrations higher than 15 μM, whereas the highest concentration tested – 100 μM affected almost all cells (4.592 ± 1.62% viable cells). The IC_{50} value calculated for AgNPs was 70.81 μM (Fig. 6). The B16Ova cells seemed to be less sensitive to the effect of AgNPs-B; the calculated IC_{50} value was 20.26 μM, a value higher as compared to the IC_{50} value recorded for betulin (3.89 μM), even though the media percentages of viable cells at low concentrations – 0.5 and 1 μM were more reduced as compared to the ones recorded for B16 melanoma 4A5 cells (0.5 μM: 95.176 ± 3.88 *vs.* 53.125 ± 3.64 and 1 μM: 62.163 ± 4.02 *vs.* 49.503 ± 6.85, respectively). AgNPs induced a decrease in living cells percentage in the case of B16Ova cells similar to the one recorded for B16 melanoma 4A5 cells, the calculated IC_{50} value was 73.07 μM with a significantly reduced percentage of viable cells at 100 μM (6.75 ± 2.99% viable cells) (Fig. 6).

PEGylated formulation of AgNPs-B induced a significant reduction of both B16 melanoma 4A5 and B16Ova living cells percentage with

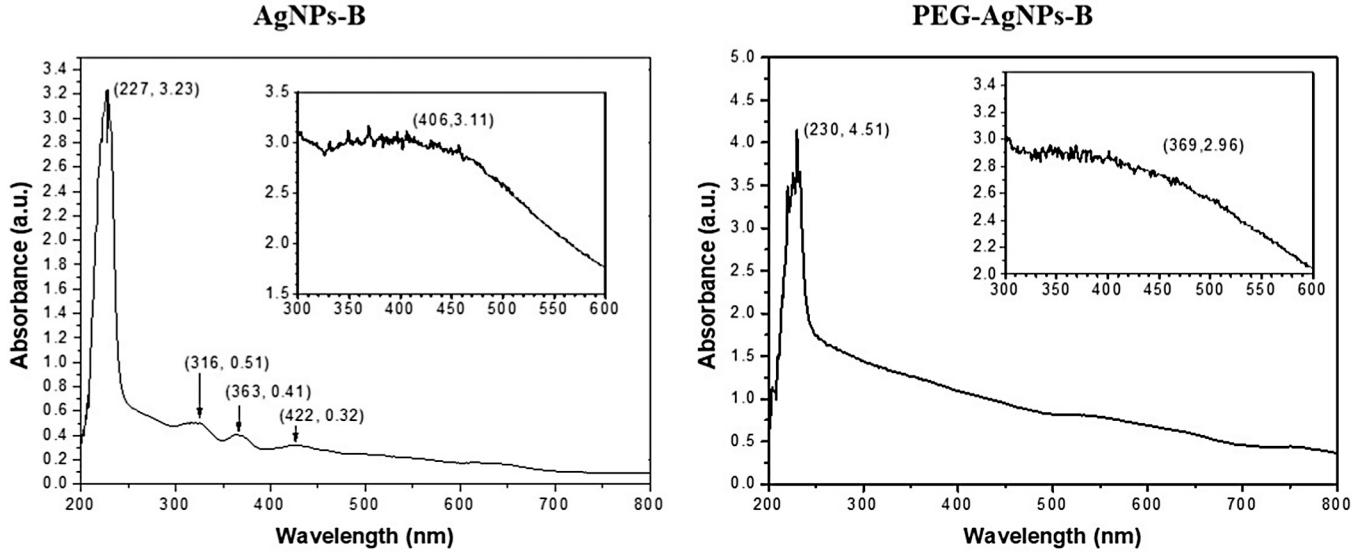

Fig. 3. UV–Vis absorbance spectra of diluted colloid samples (1:10 v:v in water) obtained with a Cary 60 UV–Vis spectrophotometer (600 nm min^{-1} scan rate). Insets show the 300–600 nm spectral range with no dilution.

Table 1
Tentative assignments of fingerprint Raman bands of colloidal betulin silver nanoparticles compared to the literature.

Experimental Raman modes (cm^{-1})	Samples	Literature Raman Shift (cm^{-1})	Tentative assignment
238–243	AgNPs, AgNPs-B, PEG-AgNPs, PEG-AgNPs-B	242 [24]	AgsbnCl, AgsbnO
756–760	AgNPs, AgNPs-B, PEG-AgNPs	739 [24]	COO^- bend
894–901	AgNPs-B, PEG-AgNPs, PEG-AgNPs-B	883 [26,27]	CsbnH deformation
924–933	AgNPs-B, PEG-AgNPs, PEG-AgNPs-B	910 [24], 913 [25]	CH_2, CH_3 rocking
1015–1022	AgNPs-B, PEG-AgNPs-B	1018 [25], 1017 [26]	$\rho(CH_3) + \rho(CH_2) + \tau\ (C_{16}H_{20}H_{21}) + \delta(CH)$
1375–1384	AgNPs-B, PEG-AgNPs, PEG-AgNPs-B	1367, 1373 [24]	CH_2 bend, $\nu_s(COO)$
1534–1548	AgNPs-B, PEG-AgNPs-B	1524 [26]	−COOH
1599–1603	PEG-AgNPs-B	1606 [24]	C=C stretch
1631–1639	AgNPs-B, PEG-AgNPs	1636 [24]	C=O stretch
1703–1717	AgNPs-B, PEG-AgNPs, PEG-AgNPs-B	1705 [24]	COO^-stretch
2808–2810	AgNPs-B	2800 [28]	C−H stretch

IC_{50} values of 2.47 μM and 5.74 μM, respectively (Fig. 7). These results indicate a stronger effect of PEG-AgNPs-B against B16Ova cells as compared to AgNPs-B formulation (IC_{50} values: 5.74 *vs*. 20.26 μM), and a similar one in comparison with betulin (IC_{50} value = 3.89 μM). In the case of B16 melanoma 4A5 cells both formulations were more potent than betulin (0.9301 and 2.47 *vs*. 4.269 μM). The dose-response tests revealed a dose-dependent decrease of cell viability, statistically significant effects being observed even at the lowest concentration used – 0.5 μM (Fig. 7). In the case of bare PEG-AgNPs, the 72 h stimulation decreased considerable the viability of both B16 melanoma 4A5 and B16Ova cells in a dose-dependent manner, the calculated IC_{50} values were 28.44 and 17 μM, respectively (Fig. 7).

The impact of test compounds (AgNPs-B, AgNPs, PEG-AgNPS-B and PEG-AgNPs) on cellular viability was also checked in two healthy human cell lines: HaCat – human keratinocytes and HEMa – primary human melanocytes, both of these cell types being strongly connected with the development of melanoma [29]. Our findings indicate that concentrations higher than 15 μM of AgNPs-B were associated with a significant decrease of living cells percentage both in the case of HaCat and HEMa cells; the calculated IC_{50} values were: 39.73 and 25.72 μM, respectively (Fig. 8). AgNPs formulations exerted a strong reduction (over 50%) of cells viability starting with 30 μM in the case of HEMa cells and at 50 μM for HaCat cells, which indicates a susceptibility of human melanocytes to AgNPs. The highest concentration used – 100 μM of all test compounds led a very low percentage of viable cells both for HaCat (around 10%) and HEMa cells (< 1%) (Fig. 8). It was

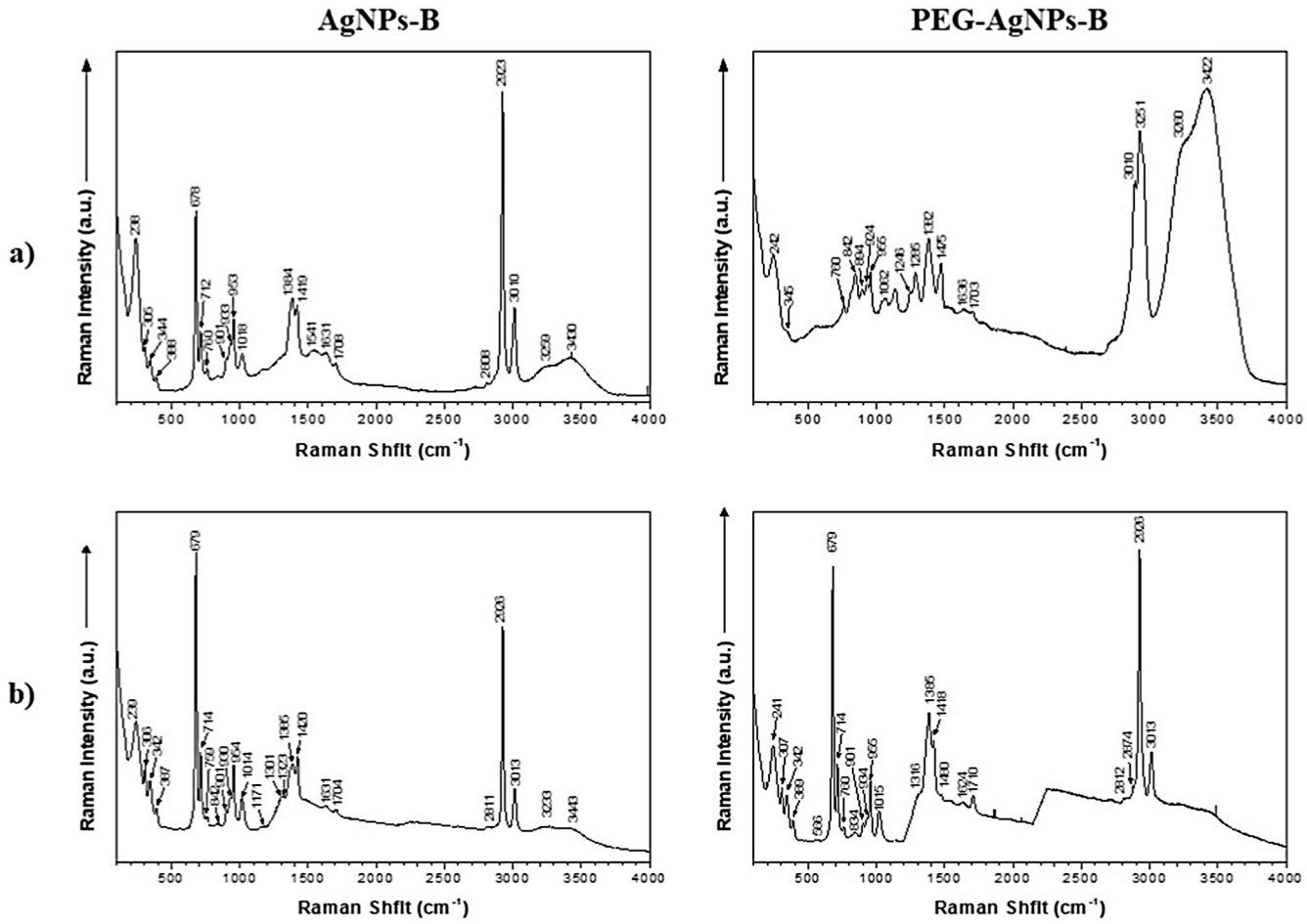

Fig. 4. Raman spectra of the colloidal samples acquired with a LabRam HR 800 Raman spectrometer using a 532.134 nm Nd:YAG (a) and 632.8 nm He-Ne (b) excitation laser and a 20 s acquisition scan averaged over 3 cycles.

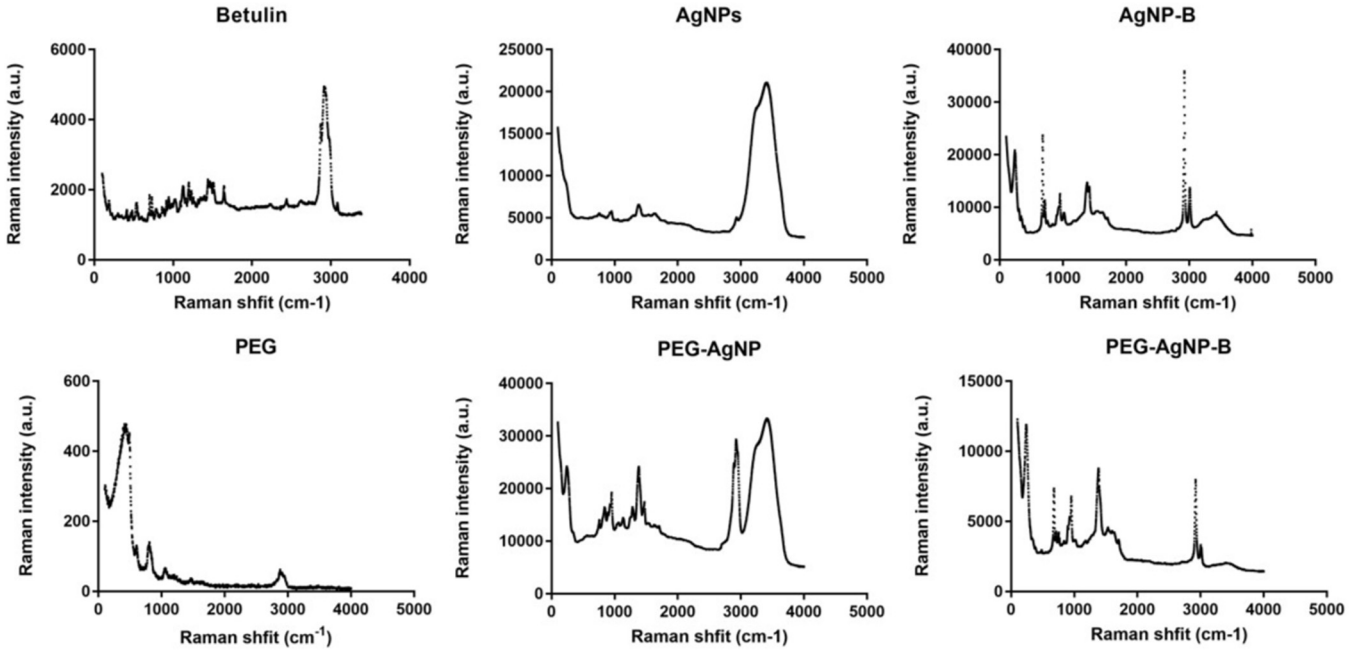

Fig. 5. Raman spectra of free betulin, betulin-loaded, bare and PEGylated silver nanoparticles.

Table 2
Drug loading capacity for betulin-loaded, bare and PEGylated silver nanoparticles.

Drug-nanoparticle ratio (w:w)	LC % (direct method)	LC % (indirect method)
AgNPs-B 1:1	51.7 ± 2.35	53.9 ± 1.67
PEG-AgNPs-B 1:1	57.6 ± 1.23	59.5 ± 1.47

also verified the effect exerted by betulin on HaCat and HEMa cells viability after a 72 h exposure, and the results indicate a significant decrease of viability rate at concentrations > 30 μM, at the highest concentration – 100 μM being recorded a viability percentage lower than 6%. The IC_{50} values calculated for betulin were 24.70 μM for HaCat and 21.63 μM for HEMa, respectively, what suggests that AgNPs-B formulation was less toxic as compared with betulin.

Exposure of HaCat and HEMa cells for 72 h to PEGylated formulations of betulin showed a considerable reduction (over 50%) of viable cells percentage at concentrations > 15 μM for HEMa and > 30 μM for HaCat cells; the IC_{50} values were: 52.98 and 86.83 μM, respectively, values significantly higher as compared with the ones calculated for betulin (24.70 μM for HaCat and 21.63 μM for HEMa) what indicates a reduced toxicity of PEG-AgNPs-B formulation related to betulin (Fig. 9). The lowest percentage of viable cells was recorded at the highest concentration used – 100 μM, and HEMa cells were found to be more sensitive to the effect of the betulin PEGylated formulations than the HaCat cells (8.852 ± 1.49 *vs*. 17.995 ± 1.34%). Bare PEG-AgNPs also presented a significant drop in HaCat and HEMa cells viability (%) at the highest concentrations used (30, 50 and 100 μM), the IC_{50} values were: 31.77 and 39.73 μM, respectively (Fig. 9).

3.3. *Pro-apoptotic effects of bare and betulin-loaded PEG AgNPs on melanoma cells*

In view of the results mentioned above indicating that PEGylated formulation of betulin was more effective in decreasing melanoma cells viability and less toxic against healthy cells (HaCat and HEMa), these formulations were characterized in terms of pro-apoptotic effects by the

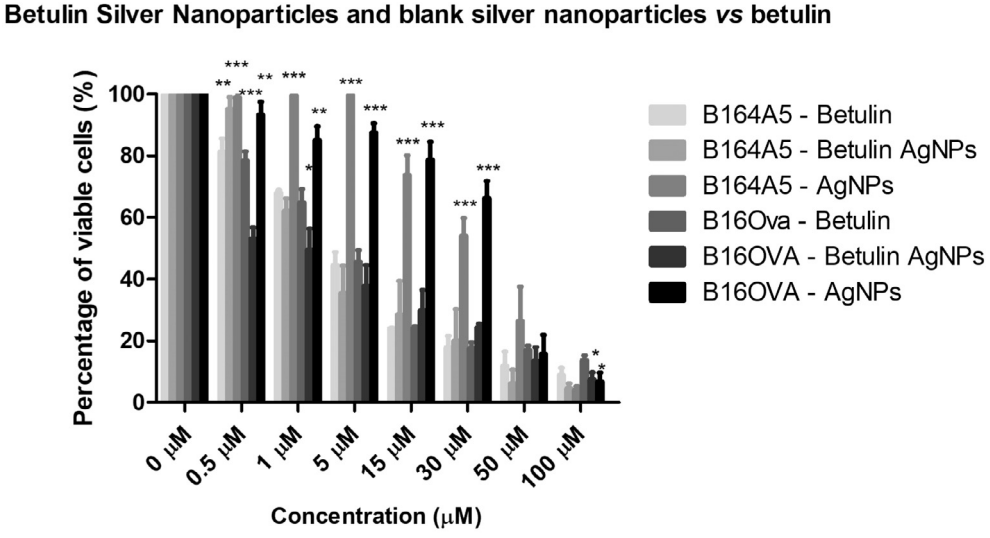

Fig. 6. *In vitro* cell viability assessment of AgNPs and AgNPs-B (0.5, 1, 5, 15, 30, 50 and 100 μM) on B164A5 and B16Ova cells at 72 h post-stimulation by MTT assay. The results are expressed as cell viability percentage (%) normalized to control cells. The data represent the mean values ± SD of three independent experiments performed in triplicate. One-way ANOVA analysis was applied to determine the statistical differences in rapport with betulin followed by Bonferroni post-test ($^{*}p < 0.05$, $^{**}p < 0.01$, and $^{***}p < 0.001$).

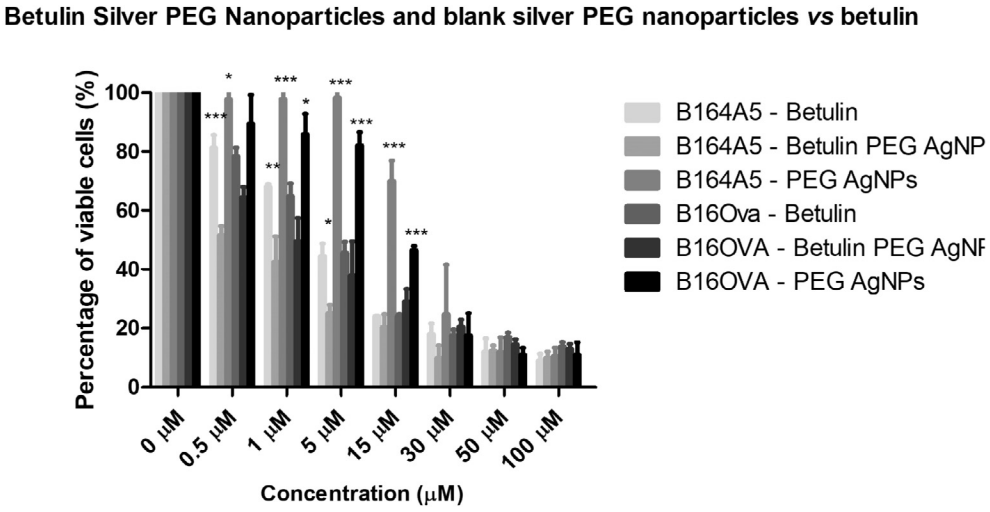

Fig. 7. *In vitro* cell viability assessment of PEG-AgNPs and PEG AgNPs-B (0.5, 1, 5, 15, 30, 50 and 100 μM) on B164A5 and B16Ova cells at 72 h post-stimulation by MTT assay. The results are expressed as cell viability percentage (%) normalized to control cells. The data represent the mean values ± SD of three independent experiments performed in triplicate. One-way ANOVA analysis was applied to determine the statistical differences in rapport with betulin followed by Bonferroni post-test ($^{*}p < 0.05$, $^{**}p < 0.01$, and $^{***}p < 0.001$).

means of flow cytometry using the Annexin V and 7-AAD as markers, which are frequently applied to differentiate viable (Annexin V negative/7-AAD negative), apoptotic (Annexin V positive/7-AAD negative), and demised (Annexin V positive/7-AAD positive) cells. As shown in Fig. 10 (lowest panel), 72 h exposure of B16 melanoma 4A5 cells to PEG AgNPs and PEG AgNPs-B caused the following events: (i) a decrease of viable cells percentage in a dose-dependent manner; (ii) a low percentage of early apoptotic cells independent of the concentrations used, and (iii) an increase in both late apoptotic (Annexin V and 7-AAD double positive) and necrotic cells populations.

The findings concerning the pro-apoptotic potential of PEG-AgNPs-B on B16Ova cells (cells that express at their surface SIINFEKL as antigen providing OVA peptide-loaded major histocompatibility complex class I molecules) are displayed in Fig. 11. The highest concentration of PEG-AgNPs-B, namely 100 μM, induced a high number of total apoptotic cells. For the other concentrations (0.5, 1, 5, 15, 30 and 50 μM) the number of total apoptotic cells was linear (dose-dependent), but the values were lower in comparison with B16 melanoma 4A5 cells. The observations noted in the case of B16 melanoma 4A5 remain valid for B16Ova cells, like: (i) a decrease in the number of viable cells in a dose-dependent manner; (ii) very low percentages of early apoptotic cells, and (iii) dose-dependent high percentages of late apoptotic and necrotic cells, with the mention that PEG-AgNPs-B proved to be active as a pro-apoptotic agent against B16 melanoma 4A5 cells.

3.4. B16 melanoma inoculation in vivo: non-invasive measurements

Non-invasive measurements were performed to monitor the physiological skin parameters (melanin content, erythema and skin hydration) changes during the *in vivo* experiment conducted on C57BL/6J mice inoculated subcutaneously with B16 melanoma 4A5 cells. The differences within parameters values were depicted in Fig. 12.

A significant difference was recorded in terms of melanin values between the control group (group 1) and the other groups of mice, in the range of 90–340 units on a 1000 arbitrary units' scale; the highest values being observed at the mice inoculated with B16 melanoma 4A5 cells and without treatment (group 2) (Fig. 12 – (a)). Quantification of erythema showed that group 4 (inoculated mice treated with PEG-AgNPs-B formulation) presented the lowest values, whereas in the case of group 2 (inoculated mice without treatment) and group 3 (inoculated mice treated with PEG-AgNPs) the values were significantly high as compared to control group – group 1 (Fig. 12 – (b)). The measurements for *stratum corneum* hydration indicated an inverse ratio to erythema, the lowest values being recorded in group 2 (inoculated mice without treatment). A decrease of hydration status was also observed in groups 3 and 4, but it was not statistically significant (Fig. 12 – (c)).

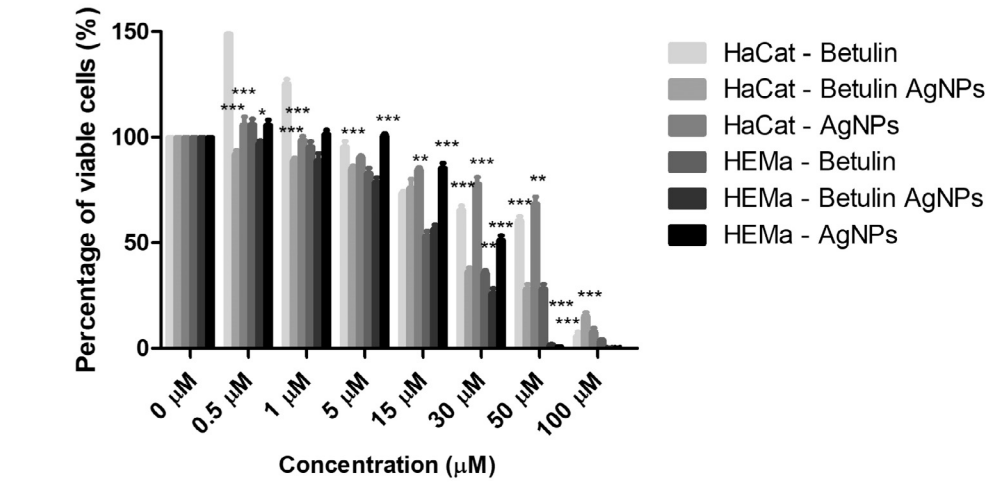

Fig. 8. *In vitro* cell viability assessment of AgNPs and AgNPs-B (0.5, 1, 5, 15, 30, 50 and 100 μM) on HaCat and HEMa cells at 72 h post-stimulation by MTT assay. The results are expressed as cell viability percentage (%) normalized to control cells. The data represent the mean values ± SD of three independent experiments performed in triplicate. One-way ANOVA analysis was applied to determine the statistical differences in rapport with betulin followed by Bonferroni post-test ($^{*}p < 0.05$, $^{**}p < 0.01$, and $^{***}p < 0.001$).

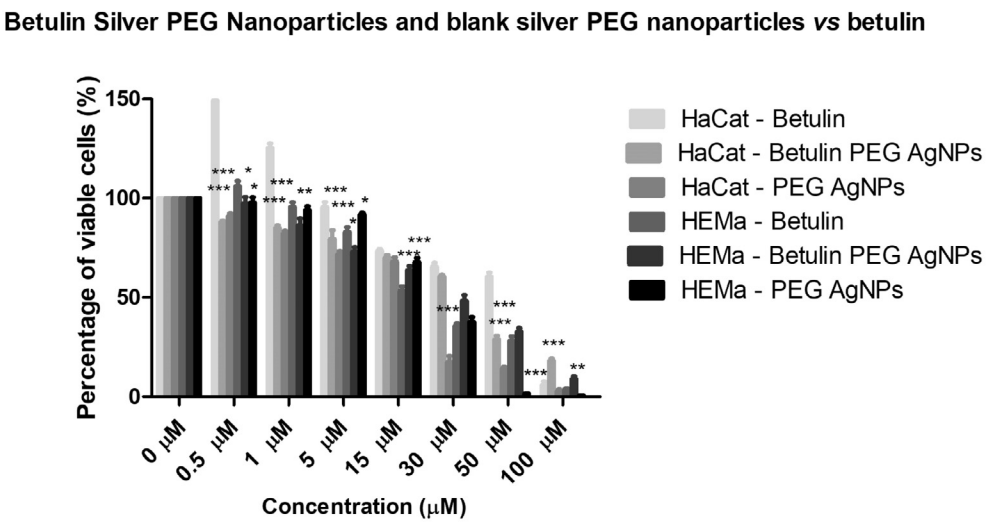

Fig. 9. *In vitro* cell viability assessment of PEG-AgNPs and PEG AgNPs-B (0.5, 1, 5, 15, 30, 50 and 100 μM) on HaCat and HEMa cells at 72 h post-stimulation by MTT assay. The results are expressed as cell viability percentage (%) normalized to control cells. The data represent the mean values ± SD of three independent experiments performed in triplicate. One-way ANOVA analysis was applied to determine the statistical differences in rapport with betulin followed by Bonferroni post-test ($^{*}p < 0.05$, $^{**}p < 0.01$, and $^{***}p < 0.001$).

3.5. Histopathological evaluation

Skin specimens from control mice showed normal epidermal and dermal architecture (Figs. 13, 1b) with some mast cells filled with basophilic granules disposed in the superficial dermis and in the perifollicular areas of reticular dermis (Figs. 13, 1a). Kidneys specimen from control mice showed minimal hyperemia of corpuscle and of peritubular capillaries (Figs. 13, 2a and b). Lungs showed minimal thickening of interalveolar septum (Figs. 13, 3a) and small quantity of inflammatory infiltrate in bronchial walls (Figs. 13, 3b). Liver specimens presented chromophobe vacuoles in hepatocytes, hyperemia of centrilobular venules (Figs. 13, 4b) and small quantity of inflammatory infiltrate in portal spaces (Figs. 13, 4a). Heart presented interstitial edema between striated cardiac muscle cells and hyperemia of small blood vessels (Figs. 13, 5a and 5b). Spleen specimen examinations revealed normal distribution of white and red pulp, with many megakaryocytes and hemosiderin laden macrophages (Figs. 13, 6a and b).

In the group 2 – mice inoculated with B16 melanoma 4A5 – a tumor was observed in the dermis and subcutis at the end of the experiment; it was ulcerated (Figs. 14, 1) and presented satellite nodules (Figs. 14, 2). The malignant melanocytes were epithelioid (Figs. 14, 3–5) and contained variable amounts of melanin. Between malignant cells, areas of necrosis (Figs. 14, 5) and many hyperaemiated blood vessels were noted (Figs. 14, 6). There were also observed mast cells filled with basophilic granules, lymphocytes and macrophages at the invasion front. No neutrophils and eosinophils were noted between or around tumor islands (Figs. 14, 7–10). In the tissue surrounding the tumor but predominantly around the deep seated vascular plexus, many inflammatory cells were observed, especially neutrophils (Figs. 14, 11–12).

Kidney collected from group 2 showed minimal deviation compared to those belonging to the control group (Figs. 15, 1a, 1b). Spleen showed hyperplasia of red pulp and many megakaryocytes (Figs. 15, 2). Lungs presented small quantities of inflammatory infiltrate in the interalveolar spaces, hyperemia of blood vessels and hemorrhagic alveolitis (Figs. 15, 3). Heart specimens exhibited tumor emboli in the cardiac cavity and some isolated pigmented malignant melanocytes in the cardiac valves and in the subendocardial layer (Figs. 15, 4a–d). Liver also displayed inflammatory infiltrates composed of similar quantity of lymphocytes and macrophages were noted around centrilobular venules and, also in portal space (Figs. 15, 5a, b); hepatocytes contained intracytoplasmic chromophobe vacuoles similar to the control group (Figs. 15, 5c). Very rare cells containing intracytoplasmic brown pigment were interpreted as metastases (Figs. 15, 5d).

In group 3, that included mice inoculated with B16 melanoma 4A5 cells and treated with PEG-AgNPs, the tumor islands were not compacted as observed at previous group (Figs. 16, 1). The tumor was composed mainly of epithelioid cells, but large areas of fusiform cells were observed for the first time during the experiment (Figs. 16, 2–3). The tumor cells contained higher amount of melanin as also observed in group 2 (Figs. 16, 4). Even so, the tumor cells still presented atypical mitosis (Figs. 16, 5). The average mitosis number on microscopic field at high power was two. Moreover, the areas of necrosis were bigger (Figs. 16, 6). Around the tumor, the mast cells were noted (Figs. 16, 7). Inflammatory infiltrate contained neutrophils, lymphocytes and macrophages at group 2 also, and the plasma cells were noted for the first time (Figs. 16, 8–9).

Liver presented moderate quantities of inflammatory infiltrate around centrilobular venules and none in portal space (Figs. 17, 1a and b). No chromophobe vacuoles were observed in the hepatocytes. Lung exhibited more inflammatory infiltrate than the other groups. The interalveolar spaces were wider (Figs. 17, 2). Kidneys showed minimal structural disruption, with slight hyperemia of corpuscle capillaries (Figs. 17, 3). Only minimal edema was observed between cardiac striated muscle, but heavy pigmented malignant melanocytes were noted in connective tissue of cardiac valve (Fig. 17, 4a–d).

The architecture of spleen seemed to be modified, with no differences between white and red pulps, because of the increased hematopoiesis in sinusoid spaces, and appearance of numerous blasts cells (Fig. 17, 5a–d).

In group 4, mice inoculated with B16 melanoma 4A5 cells and treated with PEG-AgNPs-B, the tumors were small and presented large areas of necrosis (Figs. 18, 1). The remaining tumor areas were composed of epithelioid and fusiform cells, with predominance of the epithelioid cells (Figs. 18, 2). Many malignant melanocytes showed hyperchromatic nuclei (Figs. 18, 3). Even if the tumors were smaller than in previous groups, in the remaining islands, especially in the epithelioid cells, many atypical mitoses were observed. The average mitosis number was five on microscopic field at high power (Figs. 18, 4). Around the tumor, many neutrophils, lymphocytes, and macrophages were observed (Figs. 18, 5). The number of mast cells was smaller than in the group treated with PEG-AgNPs (Figs. 18, 6).

Liver showed minimal deviation from normal histology (Figs. 19, 1a and 1b), while kidney showed normal histology (Figs. 19, 2). Heart showed a small quantity of interstitial edema between cardiac striated muscle cells (Figs. 19, 3). The spleen structure was entirely perturbed. The white pulp completely disappeared, being replaced by fibrous connective tissue. Small number of megakaryocytes was still observed, and many hemosiderin laden macrophages (Figs. 19, 4a and b). Lungs showed wide interalveolar septum and emphysema (Figs. 19, 5b). An

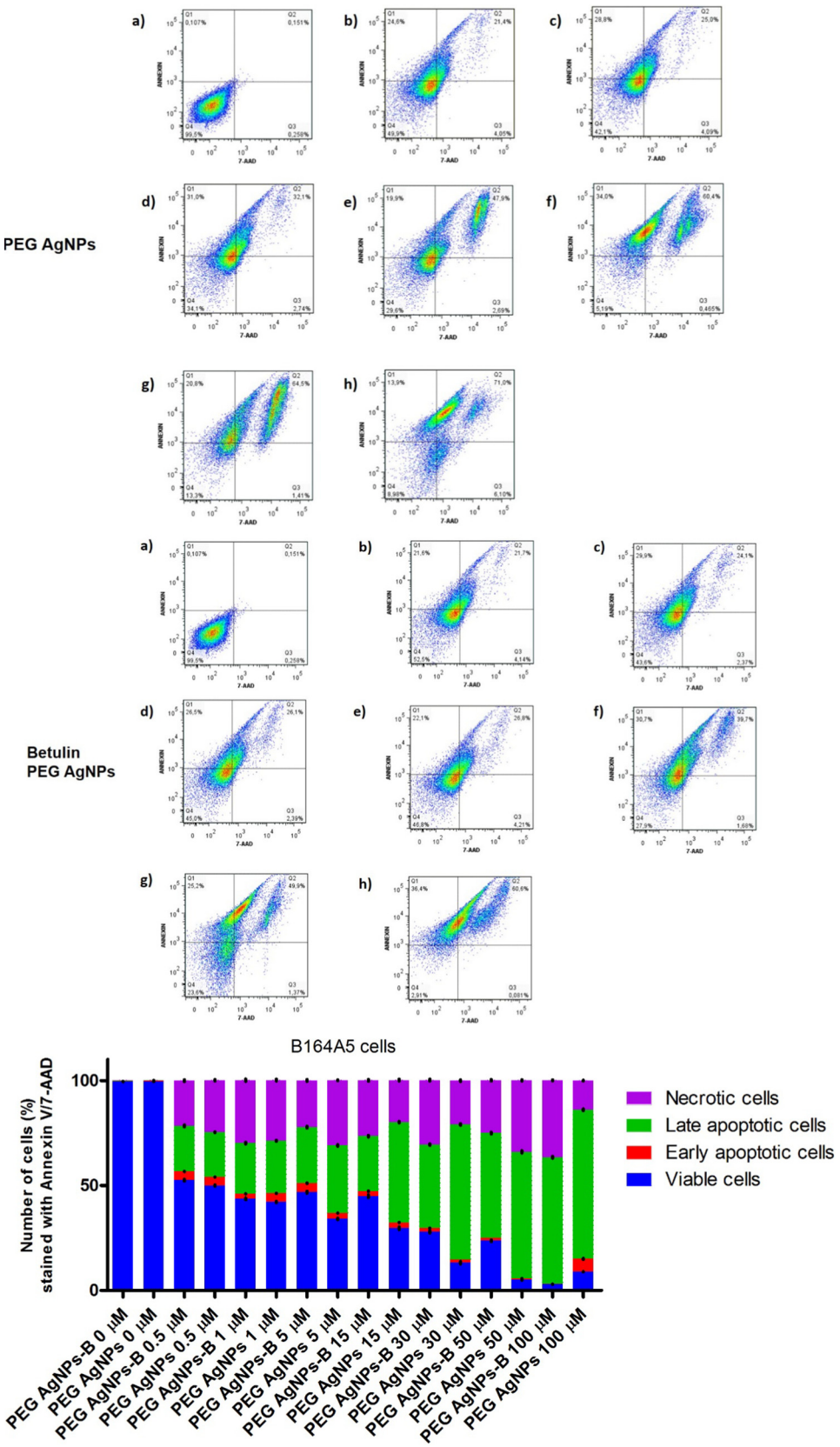

Fig. 10. Representative dot plots of the apoptotic events induced by PEG-AgNPs and Betulin PEG-AgNPs in B16 melanoma 4A5 cells after a 72 h treatment with: (a) control – 0 µM, (b) 0.5 µM, (c) 1 µM, (d) 5 µM, (e) 15 µM, (f) 30 µM, (g) 50 µM and (h) 100 µM. The cells status was analyzed by a FACS technique where: Q4 – viable cells (negative to Annexin V and 7-AAD), Q3 – early apoptotic cells (positive to Annexin V and negative to 7-AAD), Q2 – late apoptotic cells (positive to Annexin V and 7-AAD) and Q1 – necrotic cells (negative to Annexin V and positive to 7-AAD). The graph represents the percentage of B16 melanoma 4A5 in terms of: living, early apoptotic, late apoptotic and necrotic cells.

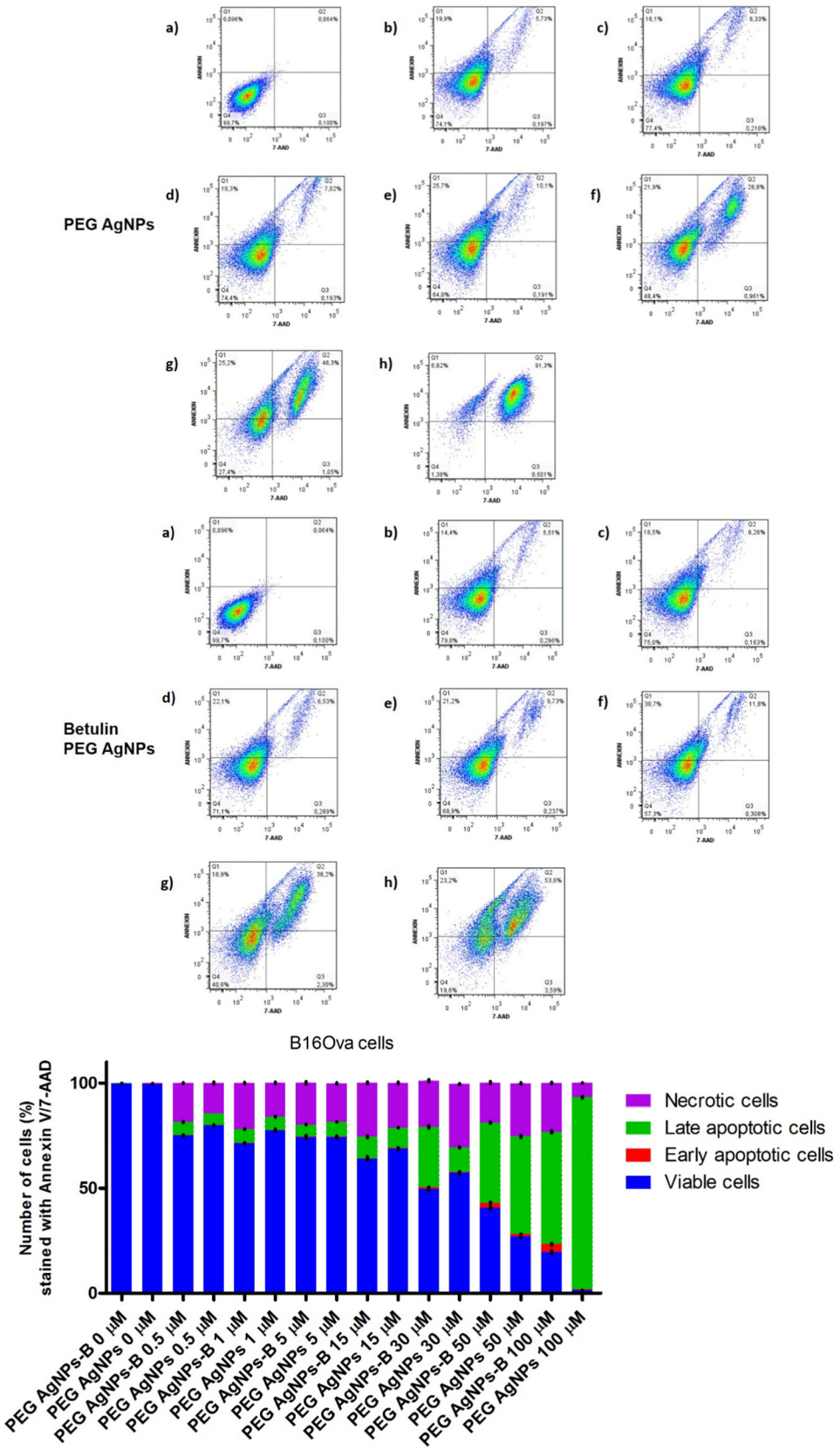

Fig. 11. Representative dot plots of the apoptotic events induced by PEG-AgNPs and Betulin PEG-AgNPs in B16Ova cells after a 72 h treatment with: (a) control – unstimulated cells (b) 0.5 µM, (c) 1 µM, (d) 5 µM, (e) 15 µM, (f) 30 µM, (g) 50 µM and (h) 100 µM. The cells status was analyzed by FACS technique where: Q4 – viable cells (negative to Annexin V and 7-AAD), Q3 – early apoptotic cells (positive to Annexin V and negative to 7-AAD), Q2 – late apoptotic cells (positive to Annexin V and 7-AAD) and Q1 – necrotic cells (negative to Annexin V and positive to 7-AAD). The graph represents the percentage of B16Ova in terms of: living, early apoptotic, late apoptotic and necrotic cells.

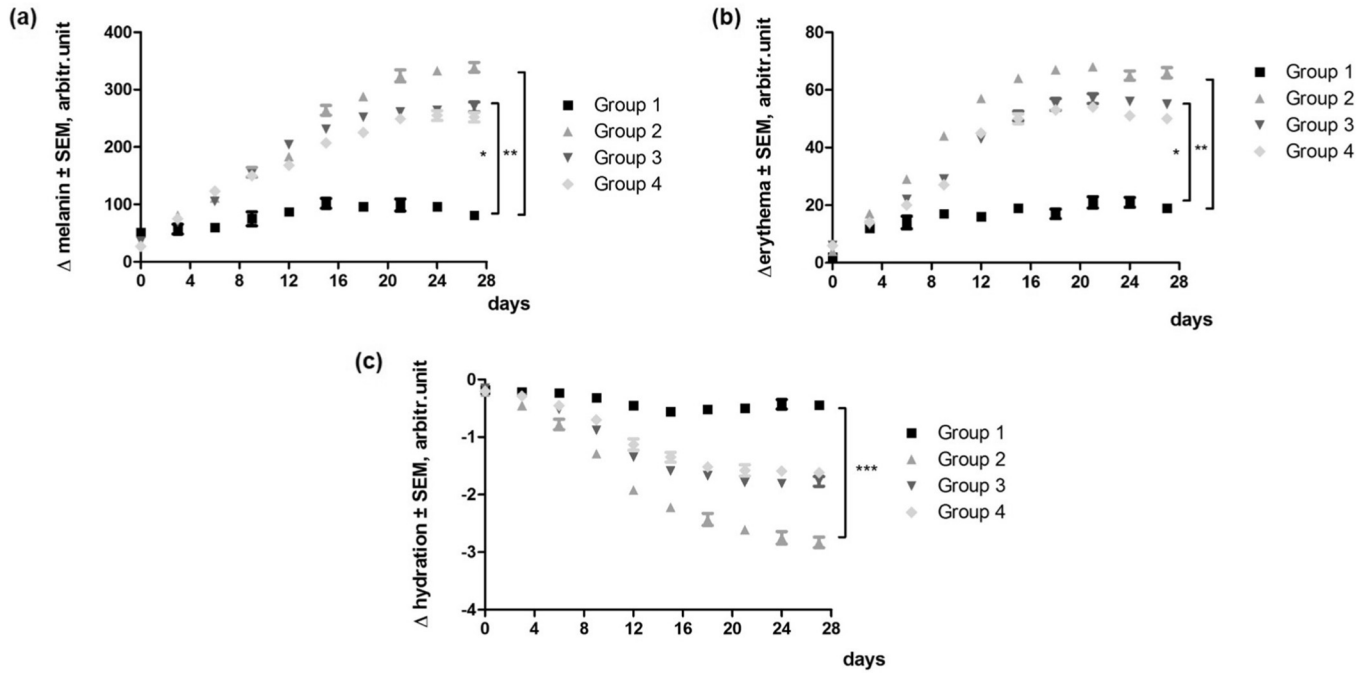

Fig. 12. Evolution of physiological skin parameters during *in vivo* experiment: (a) melanin, (b) erythema and (c) skin hydration. The data represent the mean values ± SD of three independent experiments performed in triplicate. One-way ANOVA analysis was applied to determine the statistical differences followed by Bonferroni post-test ($^{*}p < 0.05$, $^{**}p < 0.01$, and $^{***}p < 0.001$).

interesting note was the presence of some highly pleomorphic cells with monstrous nuclei replacing the alveolar cells or resting isolated in the alveolar spaces (Figs. 19, 5a).

4. Discussion

Betulin, the most abundant pentacyclic triterpene found in the outer bark of the birch tree, is known for centuries for its healing properties with a predilection on skin pathologies [30,31]. A recent study asserts the use of betulin in a randomized phase III clinical trial program, acting as an accelerator of re-epithelization process in partial-thickness skin wounds [32]. In addition, other clinical studies confirmed the effectiveness of betulin in actinic keratosis and dystrophic epidermolysis bullosa [30,33]. Albeit, betulin antineoplastic effects were proved both

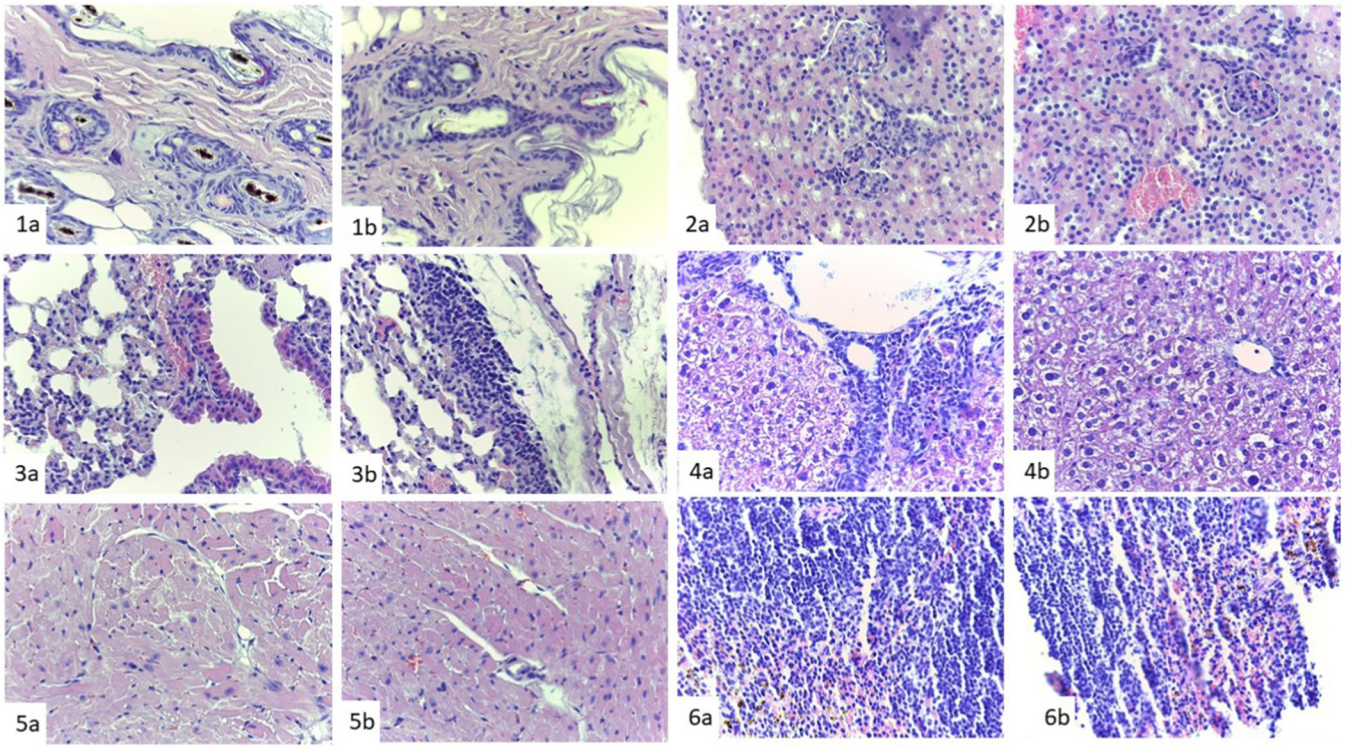

Fig. 13. Histological aspects of skin and internal organs specimens from control group mice, H&E stain.

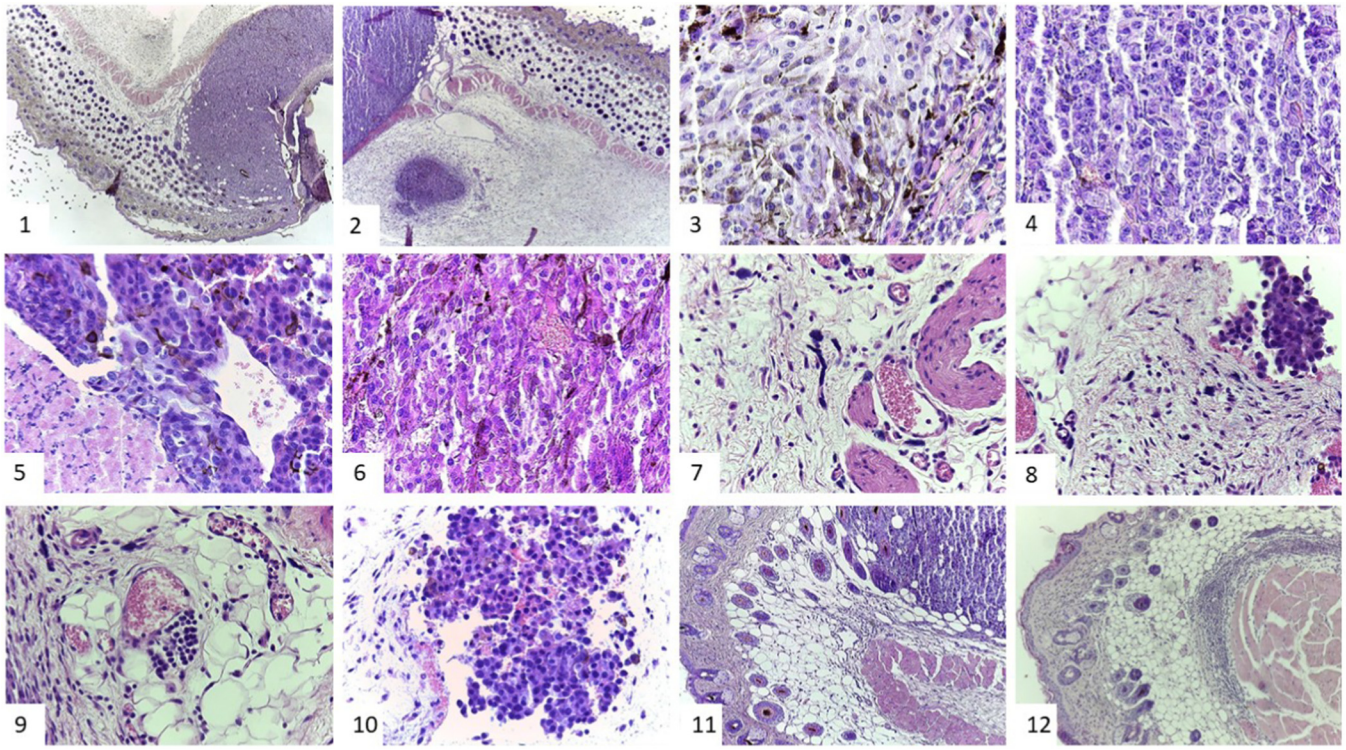

Fig. 14. Histopathological aspects of skin specimens of the mice inoculated with B16 melanoma 4A5 cells, H&E stain.

in vitro against a panel of tumor cell lines (comprehensively described in the review published by Krol et al.) [34] and *in vivo*, up to this time there are no clinical trials having as subject betulin as treatment for cancer. This major drawback is drawn by its low solubility in biological media. In recent years, a number of attempts have been made to enhance the solubility and bioavailability of betulin. Some betulin-based formulations were obtained: supramolecular complex using modified cyclodextrins (improved solubility in aqueous solutions and increased antitumor properties) [35], oil-in-water nanoemulsion (anti-angiogenic, anti-inflammatory and antitumor effects) [12], water-in-oil

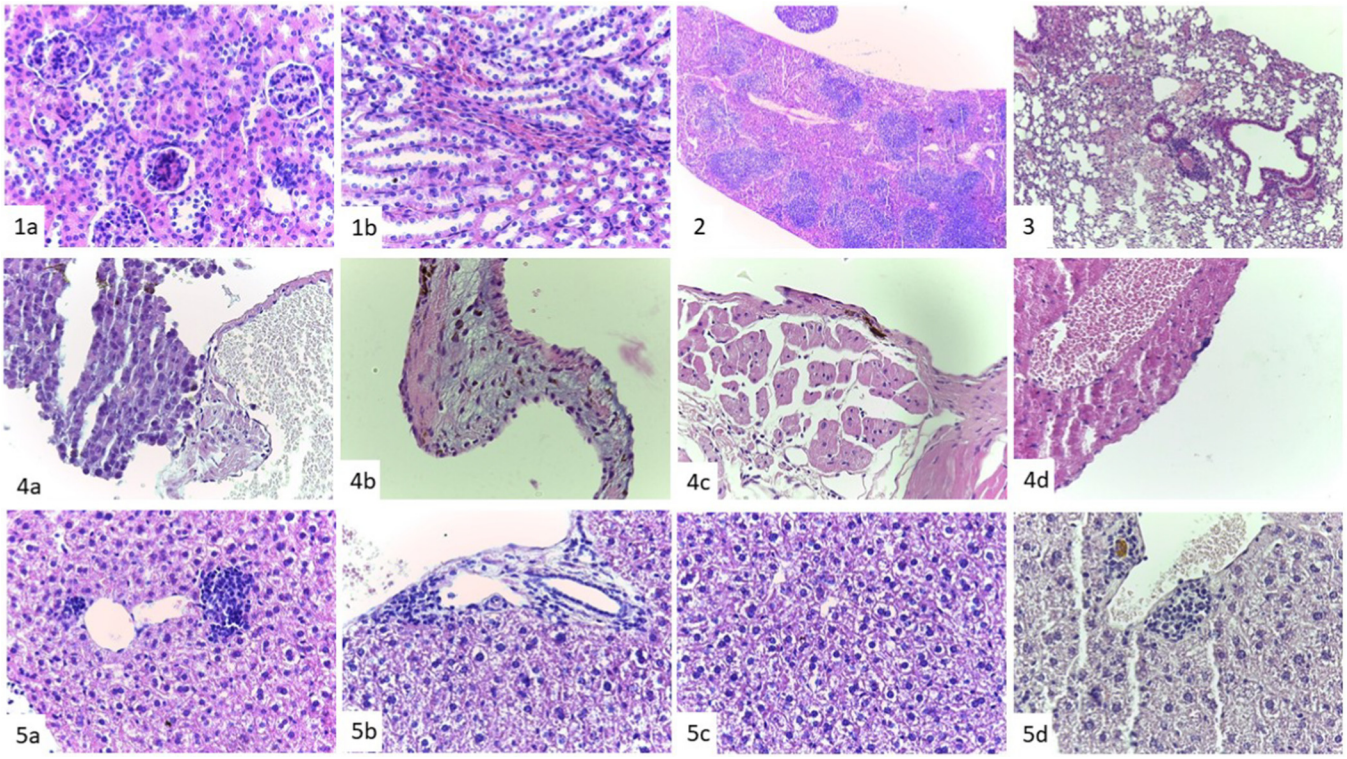

Fig. 15. Histological aspects of internal organs specimens: kidney (1a, 1b), spleen (2) and lungs (3) with minimal modifications as compared to the control group. Metastasis and tumor emboli were observed in heart (4a–d) and liver (5a–d), H&E stain.

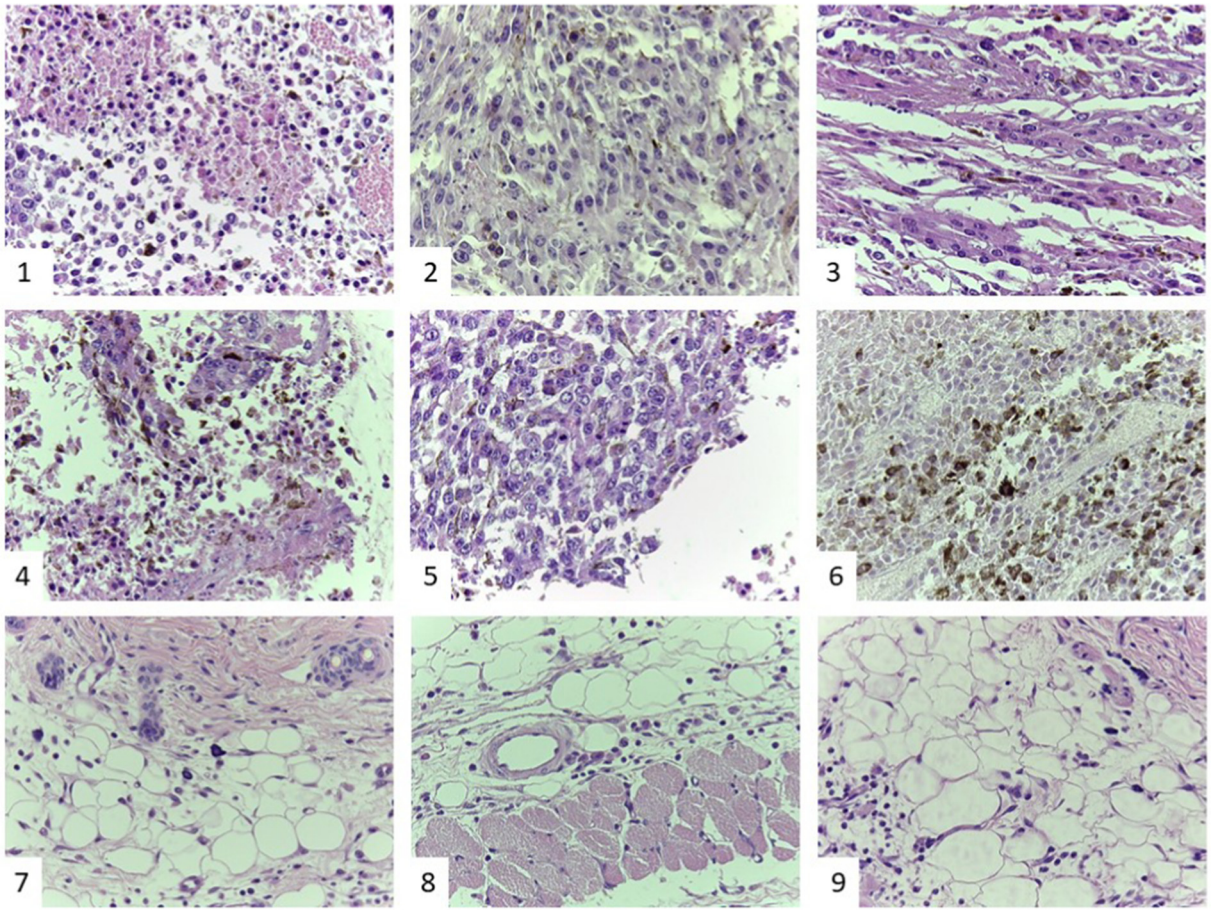

Fig. 16. Histological aspects of skin specimens of group 3 mice inoculated with B16 melanoma 4A5 cells and treated with PEG-AgNPs showed islands of dispersed cells (1). The tumor cells were mainly epithelioid, but fusiform cells were also noted (2–3). The cells presented large amount of melanin (4) and atypical mitosis (5). Large areas of necrosis were noted (6). The inflammatory infiltrate contained mast cells, neutrophils, macrophages, lymphocytes and plasma cells (7–9) (H&E stain).

foam (wound healing process) [36], poly-D,L-lactide nanovectors (PLA NVs) encapsulated with betulin (increased antitumor effect) [37], and betulin-loaded PEDOT films [38]. Nevertheless, to the best of our knowledge, there is no evidence of a stable, biocompatible formulation of betulin that improves its bioavailability and ensures its use in clinical studies.

The wide-scale applications of metallic NPs in biomedical areas unsealed new opportunities to functionalize anticancer agents for enhanced therapeutic properties and reduced toxicity. These NPs can be easily functionalized with different molecules based on their nano size and reactivity and thus can be ideal carriers for therapeutic agents [6,39]. AgNPs represent a class of nanocompounds abundantly used as anticancer agents carriers (e.g., imatinib-loaded AgNPs, noscapinoids bearing silver nanocrystals, and PEG-capped methotrexate) [40–42]. It should be noted that AgNPs also possess cytotoxic features acting as pro-apoptotic agents in different cancer cells [43–46].

On the basis of these considerations and with the scope of increasing betulin solubility in biological media, the present study synthesis bare and PEG-capped AgNPs-B formulations and evaluates these formulations in terms of: (i) *in vitro* efficacy against healthy (HaCat and HEMa) and melanoma (B164A5 and B16Ova) cells and (ii) *in vivo* antitumor properties in a murine melanoma model (using C57BL/6J mice inoculated subcutaneously with B164A5 melanoma cells).

Stable bare and PEG coated AgNPs-B of spherical shape and the mean size of 25 and 75 nm, respectively, were obtained by Turkevich's method with several modifications (previously described by Pinzaru et al.) [15]. At present, an array of methods are available for the synthesis of AgNPs (e.g., electrochemical synthesis, sonochemical method, thermal decomposition, laser ablation, chemical reduction, polyol method, microemulsion, biological synthesis using bacteria, fungus, actinomycetes, yeast and plant – mediated synthesis) [6] of desired size, shape and charge. These parameters are known to dictate their toxicological profile both *in vitro* and *in vivo*. The present study employed a one-step chemical reduction for the fabrication of stable bare and PEG-capped AgNPs of reduced *in vitro* and *in vivo* toxicity [15]. Earlier studies showed that AgNPs of sizes < 10 nm are highly toxic because of the release of Ag^+ ions, whereas AgNPs of sizes between 20 and 100 nm are less toxic and have no impact on cells integrity [14,47], this range being considered somehow a "size safe window". Our present results related to NPs size could be included in the "size safe window". The newly developed AgNPs were characterized in terms of formation (UV–Vis absorption and Raman spectra analysis), morphology and size (TEM measurements), stability (Zeta potential analysis) and drug loading capacity and encapsulation efficiency (UV–Vis measurements). Raman shifts similar to those reported in the literature by others [24,25,28] confirmed the adsorption of betulin on AgNPs and PEG-AgNPs. The shape of AgNPs is considered a key parameter in evaluating their safety profile and the spherical form was associated with a low toxicity and a reduced degree of interaction with the cells within the body [14,15]. The betulin-loaded bare and PEGylated AgNPs showed efficient and outstanding loading capacity and entrapment efficiency (~52% for AgNPs-B and ~58% for PEG-AgNPs-B), values that are similar to those reported in the literature for silver nanoparticles loaded with different active substances [22].

AgNPs are known to preserve their stability in low ionizable aqueous solutions, but neutralization of their surface may take place in the

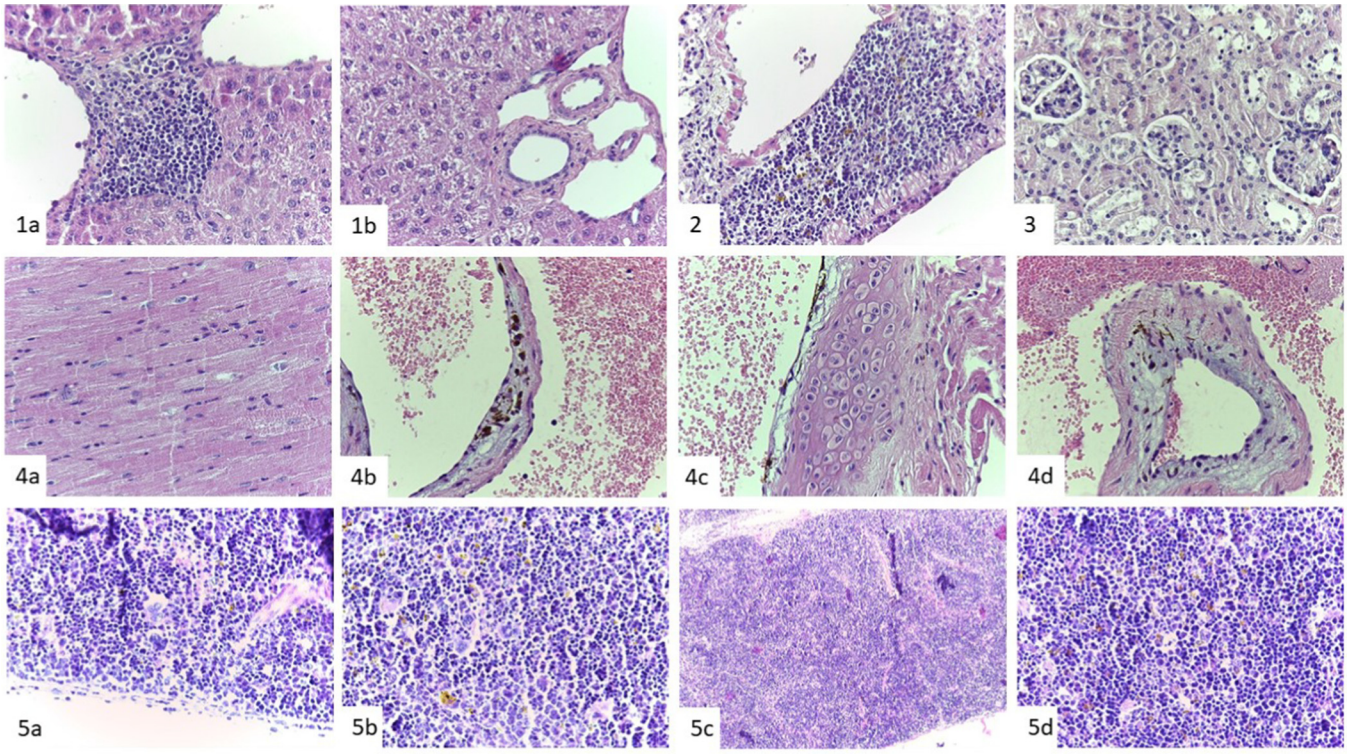

Fig. 17. Histological aspects of internal organs specimen from the group 3, mice inoculated with B16 melanoma 4A5 cells and treated with PEG-AgNPs. Liver presented inflammatory cells around centrilobular venules (1a), but not in portal spaces (1b). Lung showed wider interalveolar septa and more inflammatory infiltrate in the bronchial wall (2). Kidney specimens were similar to previous groups (3). Heart presented heavily pigmented melanocytes in cardiac valve and interatrial septa (4a–d). Spleen architecture was disturbed by hyperplasia of red pulp (5–d).

biological environment (e.g. blood, and circulating serum protein) where the ionic strength is greatly increased. This leads to the formation of aggregates predisposed to removal from the blood circulation [48]. To avoid the formation of aggregates and in order to increase the hemocompatibility and water solubility, and to decrease the cytotoxicity, their functionalization is required. PEGylation of NPs is a simple and viable solution especially due to FDA's inclusion of polyethylene glycol in the GRAS (Generally Recognized As Safe) class. Coating of NPs with PEG presents a number of advantages, such as: diminished hemotoxic properties, protection of the nucleus from the direct contact with the biological environment, enhanced solubility, improved dispersibility and minimum uptake by mononuclear phagocyte system [48–50]. Several PEGylated NPs decorated with active targeting agents are currently under clinical investigation [48]. Taking in consideration

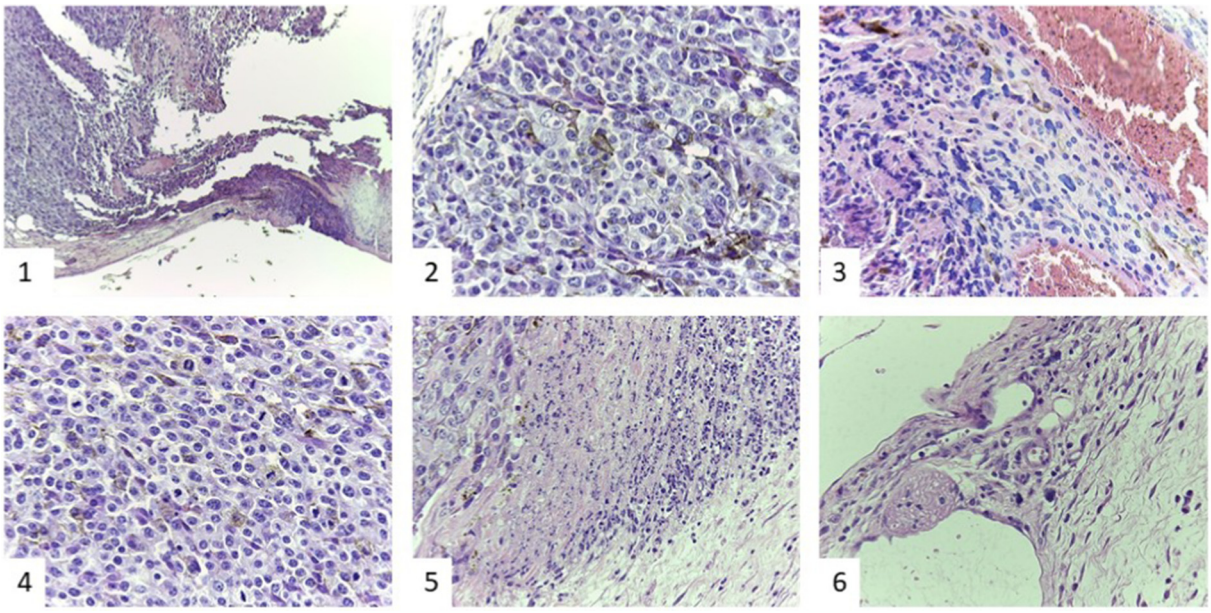

Fig. 18. Histological aspects in group 4 of mice inoculated cu B16 melanoma 4A5 cells and treated with PEG-AgNPs-B, the cutaneous tumor was ulcerated (1) and composed of epithelioid cells (2) with pleomorphic nuclei (3) and many atypical mitoses (4). Around the tumor many neutrophils, lymphocytes, macrophages and mast cells were observed (5–6) (H&E stain).

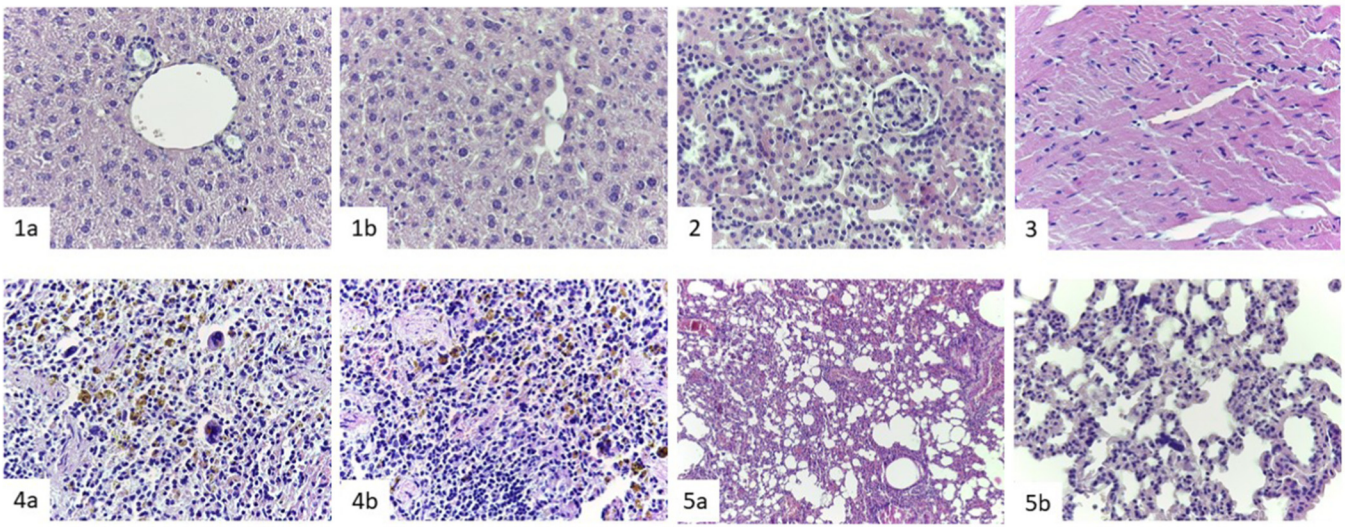

Fig. 19. Histological aspects of internal organs specimen from the group 4 of mice inoculated with B16 melanoma 4A5 cells and treated with PEG-AgNPs-B. Liver (1a and 1b), kidney (2) and heart (3) were similar to the control group. Architecture of spleen was completed perturbed and white pulp was replaced by connective tissue (4a and 4b). Lung showed wider interalveolar septum (5a) and some monstrous cells with pleomorphic nuclei lining alveolar walls (5b). H&E stain.

all these facts, polyethylene glycol was also our choice of capping agent for AgNPs-B.

The augmentation of AgNPs use in multiple biomedical fields and their potential interaction with the human body coerce a mandatory and thorough assessment of their safety. Safety profile evaluations of the test compounds (AgNPs, AgNPs-B, PEG-AgNPs, and PEG-AgNPs-B), were conducted via cell viability assays (MTT) on two healthy cell lines: human keratinocytes – HaCat and primary human melanocytes – HEMa. The HaCat immortalized cell line is an *in vitro* approved model for appraising the toxicological potential of different nanocompounds that might determine skin damage [46]. Melanocytes are a class of pigmented cells that are found in either skin or mucosal tissue, lymph nodes, and meningeal layer, which physiologically primarily arise from neural crest cells, in the epidermal layer, and are underlying melanoma occurrence [2,4,5,51,52]. Of note, keratinocytes and melanocytes are strongly bonded, because the former ones control several key processes in the melanocytes biology such as: pigment transfer, melanocytes recruitment to the epidermal melanin unit, expression of the enzymes responsible for the synthesis of melanin and transporters, biogenesis and transport of the melanosomes [53]. Our findings showed that exposure of HaCat and HEMa cells for 72 h led to a dose-dependent decrease of cells viability, with a higher susceptibility in the case of HEMa cells (Figs. 8 and 9). Moreover, PEG-AgNPs-B induced a reduced toxicity as compared to AgNPs-B (IC_{50}: HaCat: 86.83 *vs.* 39.73 μM; HEMa: 52.98 *vs.* 39.73 μM). When compared to betulin, the PEGylated formulation turned out to be also less toxic (IC_{50} values of betulin were 24.70 μM for HaCat and 21.63 μM for HEMa cells).

The toxicity of AgNPs on normal skin cell lines was also discussed by others. For example, (a) NHDF (normal human dermal fibroblasts) and NHEK (normal human epidermal keratinocytes) viability was not influenced by AgNPs (0.25–25 μg/mL) after 24 h exposure [54], (b) AgNPs applied in 0–60 μg/mL concentrations did not reduce HaCat (normal human keratinocytes) viability [55], (c) SVK 14 (human keratinocytes) and NIH 3 T3 (mouse fibroblasts) cells viability started to decrease at a concentration of 13 μg/mL AgNPs [56], (d) short exposure to AgNPs induced a persistent anti-proliferative effect in HaCat cells, and differentiation was observed in myofibroblasts [46]. Surface coating of AgNPs affected their anti-proliferative potential, namely, the coated AgNPs were found to exert toxicity in keratinocytes and melanocytes, but at a lower extent when compared to bare AgNPs, in good agreement with the literature [15,57,58]. Betulin was shown to induce differentiation of human primary keratinocytes and an apoptotic effect in senescent ones [59].

The antimelanoma potential of betulin has already been stated in human and murine melanoma cells [10,33,60], but the possible synergistic effects of AgNPs or PEG-AgNPs and betulin were not studied. Therefore, the impact of the novel formulations of betulin on two murine melanoma cell lines (B164A5 and B16Ova) was investigated. B16Ova cells were less sensitized by bare and PEGylated AgNPs-B activity in comparison to B164A5 cells. The IC_{50} value calculated for AgNPs-B was lower than that of PEG-AgNPs-B in the case of B164A5 (0.9301 *vs.* 2.47 μM), whereas for B16Ova cells, the situation was reversed, the PEGylated formulation was more active (5.74 *vs.* 20.26 μM). It should be mentioned that AgNPs and PEG-AgNPs, respectively induced a low percentage of viable cells at higher concentrations (Figs. 6 and 7). Betulin was previously reported as an active anti-proliferative agent against B164A5 cell line eliciting an IC_{50} value of 1.9 μM [1]. In the present study betulin also showed potent antimelanoma effects by reducing the viability of both B16 melanoma 4A5 and B16Ova cells (IC_{50} values: 4.269 μM – B164A5 and 3.89 μM – B16Ova cells) even at low concentrations as 5 μM (< 50% viability rate). Association with AgNPs led to an increased effect as can be seen from the IC_{50} value (0.9301 μM). The IC_{50} values (in the range of 12.4 and > 250 μM) recorded for betulin on other murine (B16-F1 and B16 2F2) and human melanoma cells (G361, SK-MEL-28, MEL-2 and SK-MEL2) [33] were significantly higher as compared with the ones obtained in the present study. This said, it can be concluded that functionalization of AgNPs and PEG AgNPs with betulin enhanced its antimelanoma activity.

Similar results were obtained when AgNPs were used as carriers of active molecules in malignant diseases: plumbagin AgNPs improved the anti-proliferative effect by enhancing the internalization of the active agent [61], doxorubicin AgNPs tremendously decreased the proliferation rate of MCF-7 and T47D human breast cancer cell lines [62], AgNPs presented an anti-proliferative potential against Hep2 laryngeal carcinoma cell line [63], AgNPs synthetized by the polyol method presented cytotoxic effects against both breast cancerous (MDA-MB-231 and MCF7) and non-cancerous (MCF 10A) cell lines [64].

Betulin was previously described as a dose-dependent pro-apoptotic agent against B164A5 and B16F10 murine melanoma cells [1]. Coating of betulin with PEG-AgNPs led to an increased apoptotic potential against B164A5 cells (Fig. 10). In a comprehensive study about the anti-proliferative and pro-apoptotic potential of AgNPs in human glioblastoma GBM cells Urbańska et al., have concluded that AgNPs are active agents eliciting both properties [65]. In case of the HepG2

human liver cancer cell line, the mechanism through which AgNPs induce apoptosis was assigned to ROS-mediated signaling pathways [66]. In a recent study, Yuan *et al.*, obtained similar results to those in this study; AgNPs enhance the apoptotic potential of gemcitabine, a consecrated anticancer drug used in different types of solid tumors such as A2780 human ovarian cancer cells [43].

Although considerable progress was recorded using the *in vitro* approaches, the mouse still remains the powerhouse for biomedical research, representing the bridge between the translational and clinical research [67,68]. The development of syngeneic models (C57BL/6 mice inoculated with B16 cell line) for gathering insights into melanoma behaviour and metastasis proved to be a useful platform by recreating an environment similar to the one found in human melanoma [69].

The present study developed a melanoma model using C57BL/6J female mice that were subcutaneously injected with B16 melanoma 4A5 cells. During the experiment, several skin physiological parameters were monitored, these include melanin content, erythema and skin hydration. Melanin is the pigment responsible for skin color and acts as a protector against epidermal carcinogenesis and malignant melanoma. Changes in melanin status may offer important clues in establishing the diagnosis of different skin pathologies, mainly melanoma [18,70]. Our data indicate an increase of melanin content in the groups inoculated with B16 melanoma 4A5 cells as compared to control, the highest increase being observed for the untreated group – group 2 (Fig. 12 – (a)). The correlation of erythema with melanin values was considered a reliable indicator for skin diseases [70]. Previous studies noted that melanoma development was accompanied by erythematous rash, also known as “Brenner sign”, which is considered a direct link to the angiogenesis process, the nutritive source for the tumor [18,71]. In this study, the highest erythema values were recorded for group 2 (untreated group) which presented the tumors with the biggest dimensions (Fig. 12 – (b)). Skin hydration elicits an important role in skin functions by controlling epidermal proliferation, differentiation and inflammation [70], a disturbance of its status being a marker for pathological signs. The lowest value for skin hydration was also observed for the untreated group (group 2), the mice from this group presenting the most critical condition. On this basis, it can be concluded that PEG-AgNPs-B had a beneficial effect on skin physiological parameters status.

There are many prognosis factors that can influence the survival rate of melanoma patients. Some of them are related strictly to the malignant melanocytes (cells morphology, intracytoplasmic melanin, and mitosis number) [52,72,73]. Other prognosis factors are represented by microenvironmental agents related to inflammatory cells that action on the malignant cells metabolism [74–76]. The third group of prognosis factors is represented by different hormones or hormones-like substances that can interact with malignant melanocytes [77,78].

Even if the melanoma cell line used it is defined as fusiform, fibroblast-like cells, the mice inoculated only with B16 melanoma 4A5 cells developed tumors composed only of epithelioid cells. The fusiform cells appeared only in the groups treated with silver nanoparticles, betulin loaded or not, the number of fusiform malignant melanocytes being bigger in the group treated with betulin loaded AgNPs. It has been previously shown that cells morphology could be considered a prognostic factor, the fusiform cells composed tumors having a better prognosis [52,73]. The changes in the cells morphology under AgNPs action, from epithelioid cells to less aggressive fusiform cells, could be considered as a benefic response at AgNPs treatment, a response that is significant in the presence of betulin.

The quantity of intracytoplasmic melanin it is also an important prognosis factor how we previously shown [52,72,73]. B16 melanoma 4A5 cells have the ability to produce melanin. The amount of melanin increased from the group inoculated only with malignant cells to the group treated with PEG-AgNPs-B, fact explained by the benefic action of betulin.

Even if in the group treated with PEG-AgNPs-B, the areas of necrosis were bigger than in previous groups, the tumor was smaller, and the malignant melanocytes presented hyperchromatic nuclei and intense acidophilic cytoplasm, aspects similar with those observed at the patients with good response to the neoadjuvant chemotherapy. The high rate of mitosis between the still vivant malignant melanocytes, could be probably attributed to a newly developed genetic atmosphere that allowed malignant melanocytes to escape from the betulin action.

It is still debating if the inflammatory infiltrate has a good or a bad influence on melanoma progress [75,76]. At our groups, the components of inflammatory infiltrate varied. At the group inoculated with melanoma cells only, the inflammatory infiltrate was composed of mast cells, lymphocytes and macrophages, while in the group treated with PEG-AgNPs-B, plasma cells could be noted around tumor islands, a phenomenon considered by many authors to have a good impact on melanomas outcome. These data suggested that PEGylated betulin AgNPs developed relevant *in vivo* effects as antimelanoma agents.

5. Conclusions

Taken together, our data provide clear proof that bare and PEGylated silver nanoparticles loaded with betulin which meet the essential conditions (in terms of shape, size and stability) for a safe use in the biological environment were synthesized.

PEG-capped AgNPs-B exerted *in vitro* a high selective toxicity at low doses on murine melanoma cells (B16 melanoma 4A5 and B16Ova, with a predilection for the former cell line) and a lack of toxicity for healthy cells (human keratinocytes and melanocytes) as compared to AgNPs-B. Increased doses of PEG-capped AgNPs-B invalidated the selectivity on tumor cells, and the toxicity was present in healthy cells too. These formulations also induced a dose-dependent pro-apoptotic effect in melanoma cells. Histopathological evaluation revealed changes regarding tumor cells morphology, from epithelioid to less aggressive fusiform shape and an increase of melanin amount in the group of mice treated with PEG-capped AgNPs-B, fact explained by the antimelanoma potential of the tested compounds.

Acknowledgements

This study was financially supported by a national grant code PN-III-P2-2.1-BG-2016-0354 offered by the Romanian National Authority for Scientific Research and Innovation, CNCS-UEFISCDI. This study was performed within the Center of Genomic Medicine from the ‘Victor Babes’ University of Medicine and Pharmacy Timisoara, POSCCE Project ID: 1854, SMIS code: 48749, ‘Center of Genomic Medicine v2’, contract no. 677/09.04.2015.

Appendix A. Supplementary material

Supplementary data to this article can be found online at https://doi.org/10.1016/j.ejpb.2018.11.006.

References:

[1] K. Pfarr, C. Danciu, O. Arlt, C. Neske, C. Dehelean, J.M. Pfeilschifter, H.H. Radeke, Simultaneous and dose dependent melanoma cytotoxic and immune stimulatory activity of betulin, PLoS One 10 (3) (2015) e0118802, , https://doi.org/10.1371/journal.pone.0118802.

[2] C. Garbe, K. Peris, A. Hauschild, P. Saiag, M. Middleton, L. Bastholt, J.J. Grob, J. Malvehy, J. Newton-Bishop, A.J. Stratigos, H. Pehamberger, A.M. Eggermont, Diagnosis and treatment of melanoma. European consensus-based interdisciplinary guideline e Update 2016, Eur. J. Cancer 63 (2016) 201e217, https://doi.org/10.1016/j.ejca.2016.05.005.

[3] M.F. Cordeiro, L.P. Marmitt, A.P. Horn, Subcutaneous injection of multipotent mesenchymal stromal cells admixed with melanoma cells in mice favors tumor incidence and growth: a systematic review and meta-analysis, Arch. Dermatol. Res. 310 (3) (2018) 231–240, https://doi.org/10.1007/s00403-018-1819-7.

[4] PDQ Adult Treatment Editorial Board. Melanoma Treatment (PDQ®): Health Professional Version. 2018 Mar 22. In: PDQ Cancer Information Summaries [Internet]. Bethesda (MD): National Cancer Institute (US); 2002-. Available from: https://www.ncbi.nlm.nih.gov/books/NBK66034/.

[5] Q. Liu, M. Das, Y. Liu, L. Huang, Targeted drug delivery to melanoma, Adv. Drug.

Deliv. Rev. 17 (2017) 30197–30207, https://doi.org/10.1016/j.addr.2017.09.016.
[6] S. Singh, A. Zafar, S. Khan, I. Naseem, Towards therapeutic advances in melanoma management: an overview, Life Sci. 174 (2017) 50–58, https://doi.org/10.1016/j.lfs.2017.02.011.
[7] F.S. Hodi, S.J. O'Day, D.F. McDermott, R.W. Weber, J.A. Sosman, J.B. Haanen, et al., Improved survival with ipilimumab in patients with metastatic melanoma, N. Engl. J. Med. 363 (8) (2010) 711–723, https://doi.org/10.1056/NEJMoa1003466.
[8] J. Larkin, V. Chiarion-Sileni, R. Gonzalez, J.J. Grob, C.L. Cowey, C.D. Lao, et al., Combined Nivolumab and Ipilimumab or monotherapy in untreated Melanoma, N. Engl. J. Med. 373 (1) (2015) 23–34, https://doi.org/10.1056/NEJMoa1504030.
[9] L. Heinzerling, P.A. Ott, F.S. Hodi, A.N. Husain, A. Tajmir-Riahi, H. Tawbi, M. Pauschinger, T.F. Gajewski, E.J. Lipson, J.J. Luke, Cardiotoxicity associated with CTLA4 and PD1 blocking immunotherapy, J. Immunother. Cancer 4 (2016) 50, https://doi.org/10.1186/s40425-016-0152-y.
[10] A. Schwiebs, H. Radeke, Immunopharmacological activity of betulin in inflammation-associated carcinogenesis, Anticancer Agents Med. Chem. (2017), https://doi.org/10.2174/1871520617666171012124820.
[11] A. Falamas, C.A. Dehelean, S. Cinta Pinzaru, Monitoring of betulin nanoemulsion treatment and molecular changes in mouse skin cancer using surface enhanced Raman spectroscopy, Vib. Spectrosc 95 (2018) 44–50, https://doi.org/10.1016/j.vibspec.2018.01.004.
[12] C.A. Dehelean, S. Feflea, D. Gheorgheosu, S. Ganta, A.M. Cimpean, D. Muntean, M.M. Amiji, Anti-angiogenic and anti-cancer evaluation of betulin nanoemulsion in chicken chorioallantoic membrane and skin carcinoma in Balb/c Mice, J. Biomed. Nanotechnol. 9 (2013) 577–589, https://doi.org/10.1166/jbn.2013.1563.
[13] E. Bebenek, E. Chodurek, A. Orchel, Z. Dzierzewicz, S. Boryczka, Antiproliferative activity of novel Acetylenic derivatives of betulin against G-361 human melanoma cells, Acta Pol. Pharm. 72 (4) (2015) 699–703.
[14] L. Wei, J. Lu, H. Xu, A. Patel, Z.S. Chen, G. Chen, Silver nanoparticles: synthesis, properties, and therapeutic applications, Drug Discov. Today 20 (5) (2015) 595–601, https://doi.org/10.1016/j.drudis.2014.11.014.
[15] I. Pinzaru, D. Coricovac, C. Dehelean, E.A. Moacă, M. Mioc, F. Baderca, et al., Stable PEG-coated silver nanoparticles - A comprehensive toxicological profile, Food Chem. Toxicol. 111 (2018) 546–556, https://doi.org/10.1016/j.fct.2017.11.051.
[16] S. Budhu, J. Wolchok, T. Merghoub, The importance of animal models in tumor immunity and immunotherapy, Curr. Opin. Genet. Dev. 24 (2014) 46–51, https://doi.org/10.1016/j.gde.2013.11.008.
[17] C. Danciu, A. Falamas, C. Dehelean, C. Soica, H. Radeke, L. Barbu-Tudoran, et al., A characterization of four B16 murine melanoma cell sublines molecular fingerprint and proliferation behavior, Cancer Cell Int. 13 (2013) 13–75, https://doi.org/10.1186/1475-2867-13-75.
[18] C. Danciu, C. Oprean, D.E. Coricovac, A. Cioca, A. Cimpean, H. Radeke, C. Soica, C. Dehelean, Behaviour of four different B16 murine melanoma cell sublines: C57BL/6J skin, Int. J. Exp. Pathol. 96 (2) (2015) 73–80, https://doi.org/10.1111/iep.12114.
[19] D.M. Rommelfanger, M. Compte, R.M. Diaz, E. Ilett, L. Alvarez-Vallina, J.M. Thompson, et al., The efficacy versus toxicity profile of combination virotherapy and TLR immunotherapy highlights the danger of administering TLR agonists to oncolytic virus-treated mice, Mol. Ther. 21 (2) (2013) 348–357, https://doi.org/10.1038/mt.2012.204.
[20] K.M. Kaluza, J.M. Thompson, T.J. Kottke, H.C. Flynn Gilmer, D.L. Knutson, R.G. Vile, Adoptive T cell therapy promotes the emergence of genomically altered tumor escape variants, Int. J. Cancer. 131 (4) (2012) 844–854, https://doi.org/10.1002/ijc.26447.
[21] J. Turkevich, P.C. Stevenson, J. Hillier, A study of the nucleation and growth processes in the synthesis of colloidal gold, Discuss. Faraday Soc. 11 (1951) 55–75, https://doi.org/10.1039/DF9511100055.
[22] M. Naz, N. Nasiri, M. Ikram, M. Nafees, M.Z. Qureshi, S. Ali, A. Tricoli, Eco-friendly biosynthesis, anticancer drug loading and cytotoxic effect of capped Ag-nanoparticles against breast cancer, Appl. Nanosci. 7 (2017) 793–802, https://doi.org/10.1007/s13204-017-0615-6.
[23] D.E. Coricovac, E.A. Moacă, I. Pinzaru, C. Cîtu, C. Soica, C.V. Mihali, et al., Biocompatible colloidal suspensions based on magnetic iron oxide nanoparticles: synthesis, characterization and toxicological profile, Front. Pharmacol. 8 (2017) 154, https://doi.org/10.3389/fphar.2017.00154.
[24] A. Fălămas, C. Dehelean, N. Leopold, C. Lehene, V. Chis, S.C. Pînzaru, Anti-tumoral betulin detection by surface enhanced Raman scattering, Studia UBB Physica LV (2) (2010) 25–32.
[25] A. Fălămas, S.C. Pînzaru, C.A. Dehelean, C.I. Peev, C. Soica, Betulin and its natural resource as potential anticancer drug candidate seen by FT-Raman and FT-IR spectroscopy, J. Raman Spectrosc. 42 (2011) 97–107, https://doi.org/10.1002/jrs.2658.
[26] S.C. Pînzaru, N. Leopold, W. Kiefer, Vibrational spectroscopy of betulinic acid HIV inhibitor and of its birch bark natural source, Talanta 57 (2002) 625–631.
[27] G. Varsányi, S. Holly, T. Fargó, Vibrations spectra and normal braons of bromofluorobenzne isomers-II Bromofluorobenzne, Spectrochemica Acta. 19 (1960) 676–681.
[28] M.E. Hadri, A. Achahbar, J. El Khamkhami, B. Khelifa, V. Faivre, T.T. Cong, F. Bourioua, Vibrational Spectrosc. 64 (2013) 78–88.
[29] J.X. Wang, M. Fukunaga-Kalabis, M. Herlyn, Crosstalk in skin: melanocytes, keratinocytes, stem cells, and melanoma, J. Cell Commun. Signal. 10 (3) (2016) 191–196, https://doi.org/10.1007/s12079-016-0349-3.
[30] A. Schwieger-Briel, D. Kiritsi, C. Schempp, C. Has, H. Schumann, Betulin-based oleogel to improve wound healing in dystrophic epidermolysis bullosa: a prospective controlled proof-of-concept study, Dermatol. Res. Pract. 2017 (2017) 5068969, https://doi.org/10.1155/2017/5068969.
[31] C. Soica, D. Antal, F. Andrica, R. Babuta, A. Moaca, F. Ardelean, Lupan-Skeleton pentacyclic triterpenes with activity against skin cancer: preclinical trials evolution, in: J.N. Latosinska, M. Latosinska (Eds.), Unique Aspects of Anti-cancer Drug Development, Intech, Rijeka, 2017, pp. 87–114, , https://doi.org/10.5772/intechopen.68908.
[32] J.P. Barret, F. Podmelle, B. Lipový, H.O. Rennekampff, H. Schumann, A. Schwieger-Briel, T.R. Zahn, H.R. Metelmann, BSH-12 and BSG-12 study groups. Accelerated re-epithelialization of partial-thickness skin wounds by a topical betulin gel: Results of a randomized phase III clinical trials program, Burns 43 (6) (2017) 1284–1294, https://doi.org/10.1016/j.burns.2017.03.005.
[33] C. Huyke, J. Reuter, M. Rödig, A. Kersten, M. Laszczyk, A. Scheffler, D. Nashan, C. Schempp, Treatment of actinic keratoses with a novel betulin-based oleogel. A prospective, randomized, comparative pilot study, J. Dtsch. Dermatol. Ges. 7 (2) (2009) 128–133, https://doi.org/10.1111/j.1610-0387.2008.06865.x.
[34] S.K. Król, M. Kielbus, A. Rivero-Müller, A. Stepulak, Comprehensive review on betulin as a potent anticancer agent, BioMed Res. Int. 2015 (2015) 584189, , https://doi.org/10.1155/2015/584189.
[35] C. Şoica, C. Dehelean, C. Danciu, H.M. Wang, G. Wenz, R. Ambrus, F. Bojin, M. Anghel, Betulin complex in γ-cyclodextrin derivatives: properties and anti-neoplasic activities in in vitro and in vivo tumor models, Int. J. Mol. Sci. 13 (11) (2012) 14992–15011, https://doi.org/10.3390/ijms131114992.
[36] A. Färber, R. Daniels, Ex vivo skin permeation of betulin from water-in-oil foams, Skin Pharmacol. Physiol. 29 (5) (2016) 250–256, https://doi.org/10.1159/000448689.
[37] R. Yadav, D. Kumar, A. Kumari, S.K. Yadav, PLA nanovectors with encapsulated betulin: plant leaf extract-synthesized nanovectors are more efficacious than PVA-synthesized nanovectors, Biotechnol. Lett. 38 (2) (2016) 259–269, https://doi.org/10.1007/s10529-015-1981-3.
[38] K. Krukiewicz, M. Cichy, P. Ruszkowski, R. Turczyn, T. Jarosz, J.K. Zak, M. Lapkowski, B. Bednarczyk-Cwynar, Betulin-loaded PEDOT films for regional chemotherapy, Mater. Sci. Eng. C. Mater. Biol Appl. 73 (2017) 611–615, https://doi.org/10.1016/j.msec.2016.12.115.
[39] L.A. Austin, M.A. Mackey, E.C. Dreaden, M.A. El-Sayed, The optical, photothermal, and facile surface chemical properties of gold and silver nanoparticles in biodiagnostics, therapy, and drug delivery, Arch. Toxicol. 88 (2014) 1391–1417, https://doi.org/10.1007/s00204-014-1245-3.
[40] S.A. Sadat Shandiz, M. Shafiee Ardestani, D. Shahbazzadeh, A. Assadi, R. Ahangari Cohan, V. Asgary, S. Salehi, Novel imatinib-loaded silver nanoparticles for enhanced apoptosis of human breast cancer MCF-7 cells, Artif. Cells Nanomed. Biotechnol. 45 (6) (2017) 1–10, https://doi.org/10.1080/21691401.2016.1202257.
[41] N. Soni, K. Jyoti, U.K. Jain, A. Katyal, R. Chandra, J. Madan, Noscapinoids bearing silver nanocrystals augmented drug delivery, cytotoxicity, apoptosis and cellular uptake in B16F1, mouse melanoma skin cancer cells, Biomed. Pharmacother. 90 (2017) 906–913, https://doi.org/10.1016/j.biopha.2017.04.042.
[42] Z. Muhammad, A. Raza, S. Ghafoor, A. Naeem, S.S. Naz, S. Riaz, W. Ahmed, N.F. Rana, PEG capped methotrexate silver nanoparticles for efficient anticancer activity and biocompatibility, Eur. J. Pharm. Sci. 91 (2016) 251–255, https://doi.org/10.1016/j.ejps.2016.04.029.
[43] Y.G. Yuan, Q.L. Peng, S. Gurunathan, Silver nanoparticles enhance the apoptotic potential of gemcitabine in human ovarian cancer cells: combination therapy for effective cancer treatment, Int. J. Nanomed. 12 (2017) 6487–6502, https://doi.org/10.2147/IJN.S135482.
[44] P. Liang, H. Shi, W. Zhu, Q. Gui, Y. Xu, et al., Silver nanoparticles enhance the sensitivity of temozolomide on human glioma cells, Oncotarget 8 (5) (2017) 7533–7539, https://doi.org/10.18632/oncotarget.13503.
[45] Y.J. Choi, J.H. Park, J.W. Han, E. Kim, O. Jae-Wook, et al., Differential cytotoxic potential of silver nanoparticles in human ovarian cancer cells and ovarian cancer stem cells, Int. J. Mol. Sci. 17 (12) (2016) 2077, https://doi.org/10.3390/ijms17122077.
[46] X.F. Zhang, W. Shen, S. Gurunathan, Silver nanoparticle-mediated cellular responses in various cell lines: an in vitro model, Int. J. Mol. Sci. 17 (10) (2016) 1603, https://doi.org/10.3390/ijms17101603.
[47] A. Ivask, I. Kurvet, K. Kasemets, I. Blinova, V. Aruoja, S. Suppi, A. Kahru, Size-dependent toxicity of silver nanoparticles to bacteria, yeast, algae, crustaceans and mammalian cells in vitro, PLoS One 9 (7) (2014) e102108, , https://doi.org/10.1371/journal.pone.0102108.
[48] J.S. Suk, Q. Xu, N. Kim, J. Hanes, L.M. Ensigna, PEGylation as a strategy for improving nanoparticle-based drug and gene delivery, Adv. Drug Deliv. Rev. 99 (Pt A) (2016) 28–51, https://doi.org/10.1016/j.addr.2015.09.012.
[49] W. Ding, H. Minamikawa, N. Kameta, T. Shimizu, M. Masuda, Effects of PEGylation on the physicochemical properties and in vivo distribution of organic nanotubes, Int. J. Nanomed. 9 (2014) 5811–5823, https://doi.org/10.2147/IJN.S75604.
[50] A. D'Souza, R. Shegokar, Encapsulation and application of metal nanoparticles in pharma, in: M. Rai, R. Shegokar (Eds.), Metal Nanoparticles in Pharma, Springer International Publishing, Cham, 2017, , https://doi.org/10.1007/978-3-319-63790-7_4.
[51] M. Hyde, J. Conner, From nevi to melanoma: understanding the basics of lesions, Phys. Assist. Clin. 1 (2016) 221–231, https://doi.org/10.1016/j.cpha.2015.12.001.
[52] F. Baderca, D. Vincze, N. Balica, C. Solovan, Mucosal melanomas in the elderly: challenging cases and review of the literature, Clin. Interv. Aging 9 (2014) 929–937, https://doi.org/10.2147/CIA.S64361.
[53] C. Delevoye, Melanin transfer: the keratinocytes are more than gluttons, J. Invest. Dermatol. 134 (4) (2014) 877–879, https://doi.org/10.1038/jid.2013.487.
[54] A. Galandakova, J. Frankova, N. Ambrozova, K. Habartova, V. Pivodova, B. Zalesak, K. Safarova, M. Smekalova, J. Ulrichova, Effects of silver nanoparticles on human

dermal fibroblasts and epidermal keratinocytes, Hum. Exp. Toxicol. 35 (9) (2016) 946–957, https://doi.org/10.1177/0960327115611969.
[55] A. Rónavári, N. Igaz, M.K. Gopisetty, B. Szerencsés, D. Kovács, C. Papp, C. Vágvölgyi, I.M. Boros, Z. Kónya, M. Kiricsi, I. Pfeiffer, Biosynthesized silver and gold nanoparticles are potent antimycotics against opportunistic pathogenic yeasts and dermatophytes, Int. J. Nanomed. 13 (2018) 695–703, https://doi.org/10.2147/IJN.S152010.
[56] J. Jiravova, K.B. Tomankova, M. Harvanova, L. Malina, J. Malohlava, L. Luhova, A. Panacek, B. Manisova, H. Kolarova, The effect of silver nanoparticles and silver ions on mammalian and plant cells in vitro, Food Chem. Toxicol. 96 (2016) 50–61, https://doi.org/10.1016/j.fct.2016.07.015.
[57] V. Bastos, J.M.P. Ferreira de Oliveira, D. Brown, H. Jonhston, E. Malheiro, A.L. Daniel-da-Silva, et al., The influence of Citrate or PEG coating on silver nanoparticle toxicity to a human keratinocyte cell line, Toxicol. Lett. 249 (2016) 29–41, https://doi.org/10.1016/j.toxlet.2016.03.005.
[58] W. Su, L. Ma, S.H. Wu, W. Li, J.X. Tang, J. Deng, et al., Effect of surface modification of silver nanoparticles on the proliferation of human lung squamous cell carcinoma (HTB182) and bronchial epithelial (HBE) cells in vitro, J. Biomed. Nanotechnol. 13 (10) (2017) 1281–1291.
[59] U. Woelfle, M.N. Laszczyk, M. Kraus, K. Leuner, A. Kersten, B. Simon-Haarhaus, A. Scheffler, S.F. Martin, W.E. Müller, D. Nashan, C.M. Schempp, Triterpenes promote keratinocyte differentiation in vitro, ex vivo and in vivo: a role for the transient receptor potential canonical (subtype) 6, J. Invest. Dermatol. 130 (1) (2010) 113–123, https://doi.org/10.1038/jid.2009.248.
[60] C.M. Şoica, C.A. Dehelean, C. Peev, M. Aluas, I. Zupkó Jr, P. Kása, E. Alexa, Physicochemical comparison of betulinic acid, betulin and birch bark extract and in vitro investigation of their cytotoxic effects towards skin epidermoid carcinoma (A431), breast carcinoma (MCF7) and cervix adenocarcinoma (HeLa) cell lines, Nat. Prod. Res. 26 (10) (2012) 968–974, https://doi.org/10.1080/14786419.2010.545352.
[61] P. Appadurai, K. Rathinasamy, Plumbagin-silver nanoparticle formulations enhance the cellular uptake of plumbagin and its antiproliferative activities, IET Nanobiotechnol. 9 (5) (2015) 264–272, https://doi.org/10.1049/iet-nbt.2015.0008.
[62] A. Hekmat, A.A. Saboury, A. Divsalar, the effects of silver nanoparticles and doxorubicin combination on DNA structure and its antiproliferative effect against T47D and MCF7 cell lines, J. Biomed. Nanotechnol. 8 (6) (2012) 968–982.
[63] F.S. Rosarin, V. Arulmozhi, S. Nagarajan, S. Mirunalini, Antiproliferative effect of silver nanoparticles synthesized using amla on Hep2 cell line, Asian Pac. J. Trop. Med. 6 (1) (2013) 1–10, https://doi.org/10.1016/S1995-7645(12)60193-X.
[64] R.G. Casañas Pimentel, V. Robles Botero, E. San Martín Martínez, C. Gómez García, J.P. Hinestroza, Soybean agglutinin-conjugated silver nanoparticles nanocarriers in the treatment of breast cancer cells, J. Biomater. Sci. Polym. Ed. 27 (3) (2016) 218–234, https://doi.org/10.1080/09205063.2015.1116892.
[65] K. Urbańska, B. Pająk, A. Orzechowski, J. Sokołowska, M. Grodzik, E. Sawosz, et al., The effect of silver nanoparticles (AgNPs) on proliferation and apoptosis of in ovo cultured glioblastoma multiforme (GBM) cells, Nanoscale Res. Lett. 10 (2015) 98, https://doi.org/10.1186/s11671-015-0823-5.
[66] B. Zhu, Y. Li, Z. Lin, M. Zhao, T. Xu, C. Wang, et al., Silver nanoparticles induce HePG-2 cells apoptosis through ROS-mediated signaling pathways, Nanoscale Res. Lett. 11 (1) (2016) 198, https://doi.org/10.1186/s11671-016-1419-4.
[67] A.C. Ericsson, M.J. Crim, C.L. Franklin, A brief history of animal modeling, Mo. Med. 110 (3) (2013) 201–205.
[68] T. Denayer, T. Stohr, M. Van Roy, Animal models in translational medicine: Validation and prediction, New Horizons Transl. Med. 2 (1) (2014) 5–11, https://doi.org/10.1016/j.nhtm.2014.08.001.
[69] O.F. Kuzu, F.D. Nguyen, M.A. Noory, A. Sharma, Current state of animal (mouse) modeling in melanoma research, Cancer Growth Metastasis. 8 (Suppl 1) (2015) 81–94, https://doi.org/10.4137/CGM.S21214.
[70] A. Firooz, B. Sadr, S. Babakoohi, et al., Variation of biophysical parameters of the skin with age, gender, and body region, Sci. World J. 2012 (2012) 386936, , https://doi.org/10.1100/2012/386936.
[71] J. Mashiah, S. Brenner, Y. Pessach, V. Barak, J. Schachter, Differences in cytokine levels in melanoma patients with and without redness (Brenner sign), Anticancer Res. 29 (5) (2009) 1793–1796.
[72] F. Baderca, C. Solovan, L. Boghian, Epidemiological and morphological data of ocular melanocytic lesions, Rom. J. Morphol. Embryol. 54 (1) (2013) 77–83.
[73] F. Baderca, S. Cojocaru, E. Lazăr, C. Lăzureanu, R. Lighezan, A. Alexa, M. Raica, T. Nicola, Amelanotic vulvar melanoma: case report and review of the literature, Rom. J. Morphol. Embryol. 49 (2) (2008) 219–228.
[74] M. Neagu, C. Constantin, G.R. Dumitrascu, A.R. Lupu, C. Caruntu, D. Boda, S. Zurac, Inflammation markers in cutaneous melanoma-edgy biomarkers for prognosis, Discoveries 3 (1) (2015) e38, , https://doi.org/10.15190/d.2015.30.
[75] M. Neagu, C. Caruntu, C. Constantin, D. Boda, S. Zurac, D.A. Spandidos, A.M. Tsatsakis, Chemically induced skin carcinogenesis: updates in experimental models, Oncol. Rep. 35 (5) (2016) 2516–2528, https://doi.org/10.3892/or.2016.4683.
[76] S. Zurac, M. Neagu, C. Constantin, M. Cioplea, R. Nedelcu, A. Bastian, et al., Variations in the expression of TIMP1, TIMP2 and TIMP3 in cutaneous melanoma with regression and their possible function as prognostic predictors, Oncol. Lett. 11 (5) (2016) 3354–3360.
[77] C. Caruntu, D. Boda, C. Constantin, A. Caruntu, M. Neagu, Catecholamines increase in vitro proliferation of murine B16F10 melanoma cells, Acta Endocrinologica 10 (4) (2014) 545–558.
[78] M. Lupu, A. Caruntu, C. Caruntu, L.M.L. Papagheorghe, M.A. Ilie, V. Voiculescu, et al., Neuroendocrine factors: the missing link in non melanoma skin cancer, Oncol. Rep. 38 (3) (2017) 1327–1340, https://doi.org/10.3892/or.2017.5817.